On the linear, stratified flow past three-dimensional obstacles

by

T. Marthinsen
Institute of Mathematics
University of Oslo

Abstract

The steady flow of a two layer atmosphere past an isolated obstacle and other three-dimensional terrain is studied using linear theory. Numerical solutions are obtained, and it is studied how the static stability influences the flow near an obstacle. For example it is found that the larger the stability gradient, the larger the disturbance of the basic flow for a given obstacle. A satellite photograph of regular lee-waves along the irregular coast of western Norway is presented, and it is demonstrated that the waves are caused by a relatively large scale topography where individual mountain peaks are wiped out.

1 - Introduction

The study of airflow over three-dimensional terrain has many important applications, and yet there is not much literature on the subject. In this paper we study the problem by assuming stationary, inviscid flow, and linearizing the equations with respect to the perturbations caused by the terrain. A similar investigation has been made by Smith (1980), but in addition to the assumptions made here, he also assumes hydrostatic flow. We shall therefore have most interest in features due to non-hydrostatic flow and stability varying with height, which causes effects that do not appear in a hydrostatic approximation.

Earlier papers on this subject are mainly concerned with lee-waves far downstream of an isolated mountain, as for example, Scorer and Wilkinson (1956), Wurtele (1957), Palm (1958), Crapper (1959, 1962) and Sawyer (1962). Gjevik and Marthinsen (1978) and Marthinsen (1980) computed lee-wave patterns and compared the theory with observations.

Except for the mentioned paper by Smith (1980), very few attempts have been made to study the flow close to the obstacle. Scorer (1956) computed the flow far above the mountain but he used an incorrect boundary condition aloft. Blumen and McGregor (1976) computed the flow numerically in a work mainly concerned with wave-drag, and their result resembles some of those presented in the present paper. The authors mentioned above all used linear theories, which are no longer valid when the parameter NH_o/U, N=Brunt-Väisälä-frequency, H_o= mountain height, U = basic wind velocity, exceeds a certain value. Drazin (1961) used an expansion in $(\frac{NH_o}{U})^{-1}$ to obtain a nonlinear solution valid for large $\frac{NH_o}{U}$, and he found expressions for small vertical deviations from the

two-dimensional, horizontal, potential flow which must necessarily be the limit as $\frac{N}{U} \to \infty$.

In section 3 of the present paper we study the linear flow near the mountain in the non-hydrostatic case, and we investigate how the static stability influences the flow. In section 4 we show how the method can be used to study flow past more complex terrain formations. Section 5 is devoted to the study of lee-waves caused by different kinds of topography. A satellite photograph of lee-waves is analyzed and the calculations are compared with observations.

2 - The mathematical model

The equations

$$U\vec{v}_x = -\frac{1}{\rho_o}\nabla p - \frac{\rho}{\rho_o}g\vec{k} \tag{2.1}$$

$$\nabla \cdot \vec{v} = 0 \tag{2.2}$$

$$U\rho_x + w\frac{d\rho_o}{dz} = 0 \tag{2.3}$$

describe the steady flow of an inviscid, incompressible fluid in the Boussinesque approximation. $\vec{v}=(u,v,w)$, ρ, p are small perturbations to the velocity, density and pressure. The basic, constant wind U is in the x-direction only. The z-axis is pointing vertically upwards. $\rho_o(z)$ is the density far upstream where $\vec{v}$, ρ, p are assumed to vanish. The perturbations are due to an obstacle

$$z = H(x,y), \quad \begin{matrix} H \to 0 \\ x \to -\infty \end{matrix} \tag{2.4}$$

The displacement of a fluid particle, $\vec{\xi}=(\xi,\delta,\eta)$ is given by

$$U\vec{\xi}_x = \vec{v} \tag{2.5}$$

and a single equation for η can be derived from those above

$$\nabla^2\eta_{xx} + \gamma^2\nabla_h^2\eta = 0 \tag{2.6}$$

Here γ is the Scorer parameter, $\gamma=N/U$ where $N=(-\frac{g}{\rho_o}\frac{d\rho_o}{dz})^{\frac{1}{2}}$ is the Brunt-Väisälä frequency.

If one does not make the Boussinesque and incompressibility assumptions, (2.6) with η replaced by $[\frac{\rho_o(z)}{\rho_o(0)}]^{\frac{1}{2}}\eta$ can still be derived by neglecting a term $Uc_s^{-2}\,\partial p/\partial x$ in comparison with βv, $\beta=\frac{1}{2}(g/c_s^2-N^2/g)$, c_s = velocity of sound, and the term β^2 compared to γ^2. For a detailed derivation, see e.g. Crapper (1959).

The solution of (2.6) depends of course on the function $\gamma(z)$. A model which is quite simple, and at the same time describes most phenomena that occur in nature is a two layer model with γ constant in each layer, the larger value near the ground, see fig. 2.1. The values of γ are γ_1 and γ_2, $\gamma_1>\gamma_2$, and the height of the discontinuity in the undisturbed state is h. This is the same model as used by Scorer and Wilkinson (1956).

The boundary conditions are: $y=H(x,y)$ at $z=0$, y and p continuous at $z=h$, and when $z\to\infty$ the perturbations must vanish or when this cannot be fulfilled, we require that the wave energy caused by the mountain must radiate upwards.

To obtain a solution, the dependent variables are written as Fourier integrals

$$\eta(x,y,z) = \int_{-\infty}^{\infty}\int_{-\infty}^{\infty} \hat{\eta}(k,l,z)e^{i(kx+ly)}\,dk\,dl$$

and the equation and boundary conditions for η are

$$\frac{d^2\hat{\eta}}{dz^2} + (\frac{\gamma^2a^2}{k^2} - a^2)\hat{\eta} = 0 \qquad (2.7)$$

$\hat{\eta}$ and $\frac{d\hat{\eta}}{dz}$ continuous at $z=h$ (2.8)

$\hat{\eta} = \hat{H}(k,l)$ at $z=0$ (2.9)

$\hat{\eta} \to 0$ or outward radiation of energy — when $z\to\infty$ (2.10)

Here $a=\sqrt{k^2+l^2}$. The solution of the above problem is

$$\hat{\eta}(k,l,z) = \hat{H}(k,l)\frac{T(k,l,z)}{T(k,l,0)} \tag{2.11}$$

$$T(k,l,z) = \begin{cases} \mu_1\cos[\mu_1(z-h)]+i\mu_2\sin[\mu_1(z-h)], & z\le h \quad (2.12) \\ \mu_1\exp[i\mu_2(z-h)], & z>h \quad (2.13) \end{cases}$$

$$\mu_K = \begin{cases} \frac{a}{k}(\gamma_K^2-k^2)^{\frac{1}{2}} & |k|<\gamma_K \\ i\frac{a}{|k|}(k^2-\gamma_K^2) & |k|>\gamma_K \end{cases}, \quad K=1,2 \tag{2.14}$$

When $z\to\infty$, $\hat{\eta}\to 0$ if $|k|>\gamma_2$, and there is an outward radiation of energy when $|k|<\gamma_2$. If the mountain contours are symmetric with respect to the z-axis, the Fourier integral for η may be written

$$\eta = 4\int_0^\infty \cos(ly)\mathrm{Re}[J(l,x,z)]dl \tag{2.15}$$

where

$$J(l,x,z) = \int_0^\infty \hat{H}(k,l)\frac{T(k,l,z)}{T(k,l,0)}e^{ikx}dk \tag{2.16}$$

The integral (2.16) is split in two parts $J_A=\int_0^{\gamma_2} dk$ and $J_B=\int_{\gamma_2}^\infty dk$. The branchpoint at $k=\gamma_2$ will be discussed later. We first look at J_A.

The integrand of J_A had a singularity at $k=0$ because $\mu\to\infty$ when $k\to 0$. If the path of integration is along the real k-axis towards $k=0$, however, the singularity there does no harm. It is of the form

$$\int_0^1 \sin\frac{1}{u}du \tag{2.17}$$

Here the change of variable $v=\frac{1}{u}$ replaces the above integral with

$$\int_1^\infty \frac{\sin v}{v^2}dv$$

By the same change of variable in J_A, we find that its integrand is absolutely integrable, and accordingly this contribution to η vanishes as $|x|\to\infty$ (Riemann-Lebesgues lemma).

For the z derivative of η, however, the singularity is of the form

$$\int_0^1 \frac{1}{u} \sin\frac{1}{u} du \qquad (2.18)$$

and turns into

$$\int_1^\infty \frac{\sin v}{v} dv$$

which exists, but this integrand is not absolutely integrable. Higher z derivatives of η may not be expressed as Fourier integrals.

The second integral J_B has singularities when $\gamma_2 < k < \gamma_1$. These are simple poles, due to zeros of $T(k,1,0)$, giving rise to trapped waves. We still assume the mountain to be the only energy source, and from the fact that the group velocity of these trapped waves is less than their phase velocity, it follows that they should be situated downstream of the mountain. This is achieved by taking the path of integration below the singularities in the complex k-plane. The path is deformed as shown on figure 2.2. J_B may now be written

$$J_B = \begin{cases} J_S^+ + J_R & x>0 \\ J_S^- & x<0 \end{cases}$$

where

$$J_S^\pm = \int_{\gamma_2}^{\gamma_2 + \infty e^{\pm i\omega}} dk$$

$$J_R = 2\pi i \sum_{k_o} \hat{H}(k_o,1) \frac{T(k_o,1,z)}{D_k(k_o,1)} e^{ik_o x}$$

$$D(k,1) = T(k,1,0)$$

and $k_o=k_o(1)$ is a (real) solution of

$$D(k_o,1) = 0 \tag{2.19}$$

The angle ω must be chosen so that the J_S-integrals exist.

It is seen that

$$J_S(1,x,z) = J_S^*(1,-x,z)$$

where the star denotes complex conjugate, and from (2.15) we find that this contribution to η is symmetric about $x=0$. Referring to J_S in the following, we mean J_S^+.

There is a branchpoint in J_p at $k=\gamma_1$. However, the sign of μ_1 drops out of the integrand, and this point causes no problem. The branchpoint at $k=\gamma_2$, on the other hand, must be treated carefully, otherwise J_S may not converge when $z>h$.

Convergence is ensured by choosing

$$\mu_2 = \frac{a}{k}(\gamma_2^2-k^2)^{\frac{1}{2}}$$

$$\arg(\gamma_2^2-k^2) \in [-\tfrac{\pi}{2},\tfrac{3\pi}{2}>$$

$$0<\omega<\tfrac{\pi}{4}$$

We argue as follows: In J_S we have $k=\gamma_2+te^{i\omega}$, t real and positive. Since

$$a^2 = 1^2 + \gamma_2^2 + 2\gamma_2 te^{i\omega} + t^2e^{2i\omega} \in [0,\tfrac{\pi}{2}>$$

$\mathrm{Re}(a)>0$, and we must have $\mathrm{Re}(\frac{a}{k})>0$, $\mathrm{Im}(\frac{a}{k})<0$. The argument of $(\gamma_2^2-k^2)$ can only be in the interval $[\pi,\frac{3\pi}{2}>$, and thus we have $\mathrm{Re}\ i(\gamma_2^2-k^2)^{\frac{1}{2}}<0$, $\mathrm{Im}\ i(\gamma_2^2-k^2)^{\frac{1}{2}}<0$. It follows that $\mathrm{Re}(i\mu_2)<0$, which ensures a negative real part of the exponent of (2.13), and thereby convergence of J_S, provided that $\hat{R}(k,1)$ does not cause any difficulties. We shall discuss this factor later.

We now conclude the procedure of computing η. It is a sum of three parts

$$\eta = \eta_A + \eta_S + \eta_R$$

with

$$\eta_A = 4\int_0^\infty \cos(ly)\left\{\mathrm{Re}\int_0^\gamma \hat{H}(k,l)\frac{T(k,l,z)}{D(k,l)}e^{ikx}dk\right\}dl \tag{2.20}$$

$$\eta_S = 4\int_0^\infty \cos(ly)\left\{\mathrm{Re}\int_0^\gamma \hat{H}(\gamma_2+te^{i\omega},l)\frac{T(\gamma_2+te^{i\omega},l,z)}{D(\gamma_2+te^{i\omega},l)}\right.$$
$$\left. e^{i\{(\gamma_2+t\cos\omega)|x|+\omega\}-\sin\omega|x|}dt\right\}dl \tag{2.21}$$

$$\eta_R = -8\pi\int_0^\infty \cos(ly)\hat{H}(k_o(l),l)\frac{T(k_o(l),l,z)}{D_k(k_o(l),l)}\sin(k_o(l)x)dl \tag{2.22}$$

where $\eta_R=0$ when $x<0$, and we have taken into account only the first mode of the solutions of (2.19). The integrals (2.20)-(2.22) may now be computed numerically. (2.22) may also be studied by asymptotic methods for large x and y, see for example, Marthinsen (1980). An asymptotic expression for (2.20) will be given in sec. 3.

The other dependent variables are computed in the same way. The only difference is a factor in the integrand. The relations between some of the Fourier transformed quantities are

$$\hat{p} = -\frac{k^2U^2}{a^2}\hat{\eta}_z \tag{2.23}$$

$$\hat{u} = \frac{k^2U}{a^2}\hat{\eta}_z \tag{2.24}$$

$$\hat{\delta} = \frac{1}{ikU}\hat{v} = -i\frac{l}{a^2}\hat{\eta}_z \tag{2.25}$$

Here δ is the displacement in the y-direction. Note how the singularity at $k=0$ enters the different J_A-integrals for η,δ,u,p. $\hat{\eta}$ is absolutely integrable, but $\hat{\eta}_z$ and accordingly δ is not. This reflects the fact that δ does not decay far downstream, as noted by Smith (1980).

Finally we specify the mountain. In section 3 we study the flow past a circular mountain, and we use

$$H(x,y) = \frac{H_o}{(1+\frac{x^2+y^2}{p^2})^{3/2}} \tag{2.26}$$

which has the simple Fourier transform

$$\hat{H}(k,l) = \frac{H_o p^2}{2\pi} e^{-pa} \tag{2.27}$$

In section 4 and 5, however, we study the flow past more complicated terrain, obtained by superposition of simple mountains. The "basic" mountain to be used there is of Gaussian shape

$$H(x,y) = H_o \exp[(-x^2-y^2)/4A^2] \tag{2.28}$$

with the Fourier transform

$$\hat{H}(k,l) = H_o \frac{A^2}{\pi} \exp[(-k^2-l^2)A^2] \tag{2.29}$$

The way of creating ridges and plateaus of different shape by superposing mountains of the type (2.28) will be explained in section 4. Neither of the choices (2.27) or (2.29) will alter the convergence properties of (2.21) as long as $\omega<\frac{\pi}{4}$.

3 - The flow near an isolated obstacle

In this section, we shall evaluate the integrals for η, i.e. the integrals (2.20)-(2.22), by Gauss quadrature and study the results. We scale the variables of dimension length with 1 km, e.g. $h=1.5$ means $h=1.5$ km, $\gamma=0.5$ means $\gamma=0.5$ km$^{-1}=0.5\cdot10^{-3}$ m^{-1}, and so on. Since we are only dealing with linear theory, the height of the mountain, H_o, only enters the results as a factor outside the integrals, and when talking about values of η, $\eta=0.1,0.2,\ldots$, we actually mean $\eta=0.1H_o,0.2H_o,\ldots$. Throughout this section we use the mountain (2.26) with $p=1.0$ when nothing else is said.

The flow is still affected by three parameters γ_1,γ_2,h that may vary independently, and we can only try to get a rough idea about the behavior of the flow for different atmospheric conditions. At the end of this section we discuss the validity of the linear theory. The conclusion there is that linear theory breaks down for small z when $\gamma_1 h$ and of course H_o exceed certain values.

The simplest atmosphere is the one obtained when $\gamma_1=\gamma_2$. Then $\eta_R=0$ and $\eta=\eta_A+\eta_S$. The contribution from η_S is symmetric about $x=0$ while η_A, which represents a field of vertically propagating waves, is not. Thus if γ is very small, so is the contribution from η_A, and the flow has nearly fore-aft symmetry. Fig. 3.1 shows contour lines of η at $z=1.0$ when $\gamma_1=\gamma_2=0.2$, and it is seen that the flow is quite symmetric. The sinking downstream is small compared to the lifting above the mountain. This cannot be described in the hydrostatic approximation which assumes $|k|>>\gamma$. The calculations of Smith (1980) therefore show only strongly asymmetric situations.

As γ increases, the flow becomes more asymmetric; there is a lifting of the air in front of the mountain, and sinking in the lee. In fig. 3.2 $\gamma_1=\gamma_2=1.0$, $z=1.0$ we see an example of this.

The flow pattern now resembles those of Smith; the flow is nearly hydrostatic. The slight sinking in the lee apparent on fig. 3.1, gets slowly broader and stronger while the lifting in front diminishes as γ increases. This is so because when the stability increases, a larger part of the flow passes to the side of the mountain rather than above. To compensate for the horisontal divergence, there is a sinking of air from above. When γ is increased even further, the linear theory will no longer be valid except for extremely small mountains. For large γ we expect to find no vertical motion, and it has been shown by Drazin (1961) that asymptotically when $\gamma\to\infty$, the flow is truely two-dimensional with potential flow (and thus fore-aft symmetry) in each xy-plane.

When $\gamma\to\infty$, we can easily find an asymptotic expression for η in our linear theory. The integral for η for large γ can be written (with $\hat{H}$ given by 2.27)

$$\eta = \frac{p^2 H_o}{2\pi} \int_{-\pi}^{\pi} \int_{o}^{\infty} e^{-pa} e^{i\gamma z/\cos\varphi} e^{ia(x\cos\varphi+y\sin\varphi)} a\,da\,d\varphi \qquad (3.1)$$

(This is the expression for η in the hydrostatic aproximation). Carrying out the a-integration, we find

$$\eta = \frac{p^2 H_o}{2\pi} \int_{-\pi}^{\pi} \frac{e^{i\frac{\gamma z}{\cos\varphi}}}{(p-i(x\cos\varphi+y\sin\varphi))^2} d\varphi$$

Since γ is large, the integrand oscillates rapidly except near stationary points of the exponent, $\varphi=0,\pi,2\pi$. Applying the method of stationary phase, we find an asymptotic expression for η

$$\eta \approx \frac{p^2 H_o}{2\pi}\left(\frac{2\pi}{\gamma z}\right)^{\frac{1}{2}} \frac{1}{(p^2+x^2)^2}\left\{(p^2-x^2)\cos\left(\gamma z+\frac{\pi}{4}\right)-2x\sin\left(\gamma z+\frac{\pi}{4}\right)\right\}+0\left(\frac{1}{\gamma z}\right) \qquad (3.2)$$

This expression describes a field of vertically propogating waves with phase fronts perpendicular to the basic flow, i.e. $\frac{\partial}{\partial y}=0$, and it has no resemblance to a real flow in the case of large γ.

Returning to moderate values of γ, we find on fig. 3.3 the result when $\gamma_1=\gamma_2=0.2$ at $z=2.0$. This is the same atmosphere as on fig. 3.2 At this higher level the disturbance has grown wider, but weaker, and it now differs less from the hydrostatic case. The reason for this is that long waves propagate faster than shorter ones, and thus the flow becomes more hydrostatic for larger z (keeping x and y constant). Consequently (3.2) is an asymptotic expression for η, valid for large z, and we find that the flow far above the mountain is independent of y.

The formula (3.2) predicts that η decay as $z^{-\frac{1}{2}}$ when $z\to\infty$. This is not correct in a real atmosphere where the density decreases with height, but we obtain the result as a consequence of having made the Boussinesque-approximation. As explained in section 2 we can avoid this approximation and then obtain the same integral for η, but this time multiplied by the factor $(\rho_0(0)/\rho_0(z))^{\frac{1}{2}}$. Thus with constant N, linear theory actually predicts an exponential increase of η as $z\to\infty$, which implies that nonlinear effects must be taken into account. This has been done in the two-dimensional case by Mobbs (1981) who by using the Generalized Lagrangian--Mean formulation found that the interaction of a single wave mode with the mean flow acts to reduce the wave amplitude, particularly at levels where the wind speed is low. With a constant basic velocity, Mobbs obtains an approximately linear increase in amplitude up to about 100 km. The linear theory works well at low levels with a 10% deviation at 10 km and for the altitudes we have most interest in here, i.e. z=1-5 km, there is no significant difference in amplitude between linear and nonlinear theory.

When $\gamma_2 < \gamma_1$ the term η_R is no longer zero. This term represents a field of trapped lee-waves, i.e. they decay exponentially when z increases above h. η_R vanishes for $x<0$, and calculations show that it is negative for small x and y, so that it contributes to the sinking behind the mountain. For large x and y the trapped lee-waves are the dominant contribution to η. These lee-waves are made up of two parts, both contained in a wedge behind the mountain. There are transverse waves with wave crests nearly perpendicular to the wind, and diverging waves with the crests more inclined to the wind. The transverse waves may be partially or completely missing. In section 5 we discuss some consequences of this. For a more detailed study of the lee-waves, see Marthinsen (1980).

We now study how the different parameters of the two layer model affect the flow near the mountain by varying one at the time. Fig. 3.4-3.7 show η at $z=h=1.0$. γ_2 is kept fixed equal to 0.2 while γ_1 takes the values 0.4, 0.6, 0.8, 1.0. It is seen that the lifting of air above the mountain gets flater and wider cross-wind as the stability increases. There is also a strong sinking behind the mountain due to the lee-waves. If we compare the effect of increasing γ_1 with an increase in both γ_1 and γ_2 ($\gamma_1=\gamma_2$), we find that the picture is roughly the same behind the mountain. This could be expected because the sinking is due to lee-waves in both cases. Whether the waves are trapped or not is unimportant near the source.

On fig. 3.8-3.11 γ_1 is fixed, $\gamma_1=1.0$, while $\gamma_2=0.0$, 0.4, 0.6, 0.8. $z=h=1.0$ as before. Note that fig. 3.7 fits in here with $\gamma_2=0.2$ and also fig.3.2 with $\gamma_2=1.0$. As γ_2 increases, the sinking area gets wider and the amplitude increases. This was also the case when γ_1 increased, and the reason is that a large

stability causes most of the air to pass to the side of the mountain instead of above. The sinking is to compensate for this horizontal divergence.

In contrast to the sinking, the lifting area above and in front of the mountain is seen to widen as γ_2 decreases. Thus the width of this area seems to depend upon the magnitude of $\gamma_1-\gamma_2$, that is the change in stability with height. The larger $\gamma_1-\gamma_2$, the further out to the sides of the obstacle will the disturbance be felt.

Now, let us keep γ_1 and γ_2 fixed, $\gamma_1=1.0$, $\gamma_2=0.2$ and vary h and z. First with z fixed, $z=1.0$, we have on fig. 3.12-3.16 $h=1.0, 1.5, 2.0, 2.5, 3.0$. It is seen that as h increases, the with of the disturbance increases to a maximum and then decreases. We also see that (roughly) the largest values of η are found in the cases when the disturbance has its largest spreading cross-stream. For these parameter values there must be much more wave-energy than for other values.

When h becomes very large, it might be expected that one obtains the same result as when $h\to\infty$, that is fig. 3.2. But this is not the case. Our computations show that as h increases, with z fixed, the downstream disturbance vanishes instead of approaching the result on fig. 3.2, see fig. 3.17 where $h=6.0$. The difference is due to the assumed steadiness of the flow. The flow has had an infinite time to develop, and thus reflection from even very large heights influences the flow. In a real situation with discontinuity of γ at a large altitude, the flow will first take the form on fig. 3.2 while energy radiates upwards. Then after a long time, the reflected waves are also fully developed and fig. 3.17 describes the flow.

Finally, fig. 3.18, 3.19, 3.20 have $\gamma_1=1.0$, $\gamma_2=0.2$, $h=2.0$, and z is 0.5, 1.5, 2.0. We note that the lifting region above the mountain vanishes quite rapidly but apart from this, nothing new is revealed here.

As mentioned earlier in this section, the linear theory we are using breaks down when z becomes small. As noted by Smith (1980) there are several criteria which can be used to indicate this breakdown. They all show that linear theory can no longer be used when the Scorer parameter multiplied with the mountain height becomes too large. The criterion that gives the smallest limit is the one that requires $\eta_z>-1$. When $\eta_z<-1$, the η-surfaces and thereby the density surfaces intersect. Smith finds that this first occurs at $z=0$ when $\gamma H_o \approx \frac{1}{2}$ (hydrostatic flow, γ constant with height). But the breakdown seems to be confined to a layer close to the ground.

This is illustrated on fig.3.21. It shows η as a function of x in the plane $y=0$ at different values of z. The thick dotted line is the ground. H_o is 1, and $\gamma_1=\gamma_2$ is larger on fig. 3.21a. We see that the η-surfaces intersect at the mountain top and for the larger stability also downstream close to the ground. On fig. 3.22 we see what the situation is like when H_o is smaller, here 0.5. There is still some intersection downstream for large γ, but only in a very thin layer.

The conclusion must be that the linear theory breakes down near the ground, but as far as the criterion used here is concerned, this is far from being violated when z is about 1 or greater for γH_o as large as 1.0. Of course viscous effects also become important near the ground, and the flow at these low levels is quite another problem than the one studied in this paper.

4 - The flow past more complex terrain

Since our equations and boundary conditions are linear, we may obtain the solution for flow past more complex terrain by superposition. The flow field generated by two or more mountain tops is simply the sum of the field generated by each of the single mountains. An example may be found in Marthinsen (1980) where the lee-waves behind the two peaks at Jan Mayen are calculated. We may also make mountain ridges and plateaus by integrating the expression for a single mountain.

Assume that the single peak is $z=H(x,y)$, H given by (2.28). Then a ridge from $y=0$ to $y=a<\infty$ is given by

$$R(x,y) = R_o \int_o^a H(x,y-t)dt / \int_o^a H(0,t)dt \qquad (4.1)$$

Here R_o is the height at the origin. A plateau above the domain $y>\alpha(x)$, $\alpha(0)=0$ (see fig. 4.1)

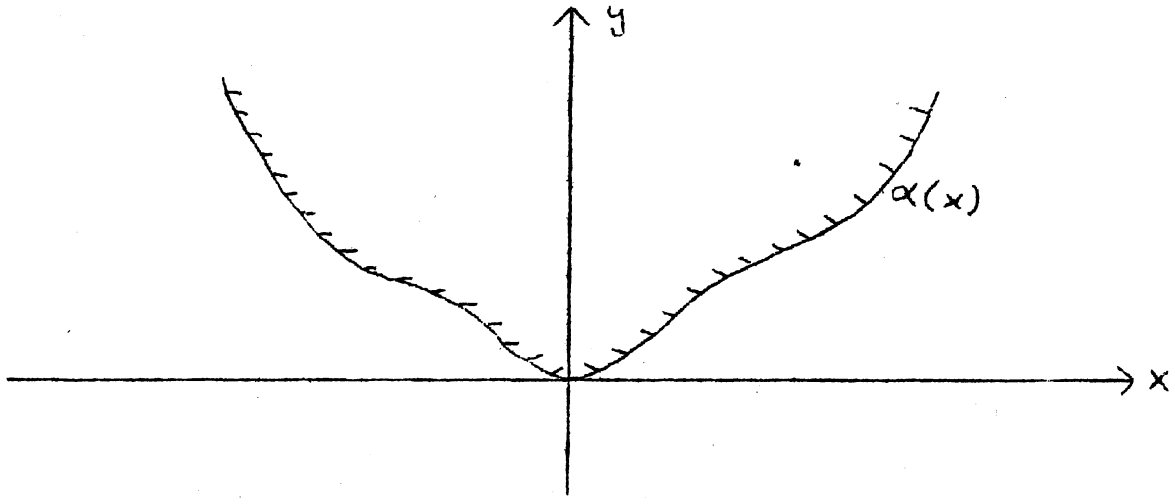

Fig. 4.1

is given by

$$P(x,y)=P_o \int_{-\infty}^{\infty} \int_{\alpha(s)}^{\infty} H(x-s,y-t)dtds / \int\int H(s,t)dtds \qquad (4.2)$$

If the displacement created by the mountain $H(x,y)$ is $\eta_H(x,y,z)$, the displacement due to $P(x,y)$ is

$$\eta_p(x,y,z) = \int_{-\infty}^{\infty} \int_{\alpha(s)}^{\infty} \eta_H(x-s,y-t,z)dtds/\int\int H(s,t)dtds$$

$$= \int_{-\infty}^{\infty} \int_{-y+\alpha}^{\infty} \eta_H(u,v)dvdu/\int\int H(s,t)dtds \qquad (4.3)$$

Inserting (2.28) in (4.1) with $a=\infty$ gives a simple ridge

$$R(x,y) = R_o e^{-\frac{x^2}{4A^2}}(1+\mathrm{erf}(\frac{y}{2A})) \qquad (4.4)$$

where erf denotes the error function

$$\mathrm{erf}(x) = \frac{2}{\sqrt{\pi}} \int_0^x e^{-t^2}dt$$

Fig. 4.2 shows the flow field near the end of the ridge (4.4). The atmospheric parameters are $\gamma_1=1.0$, $\gamma_2=0.2$, $z=h=1.0$. Thus fig. 3.7 is the same atmosphere flowing past a circular mountain. The flow past the ridge is quite similar to that computed by Smith (1980). For large y the flow becomes two-dimensional, and the figure reveals the transition between two-dimensional and three-dimensional flow. The width of the transition region is determined by the with of the wake in the case of a single peak.

5 - Lee-waves due to ridges and corners

In this section we study closer the lee-wave part of (4.3), i.e. the pole-contribution to the integral. On satellite photographs one can often see a very regular lee-wave pattern generated by a rather irregular terrain, see Gjevik (1980). Fig. 5.1 shows lee-waves along the coast of Norway. The wave system is quite regular although the mountainous area of western Norway is not. It looks as if the individual peaks are smoothed out, and the waves generated by some larger topographical structure. The wave system seems to start at Stad (the point S on fig. 5.2), and we shall demonstrate that a "corner" like the norwegian coast at Stad is able to generate a wave system as seen on the satellite photograph, fig. 5.1.

The photograph is taken at 10.00 GMT and fig. 5.3 shows the upper air data as recorded by a radiosonde released at Ørland (Ø on fig. 5.2) 11.05 GMT. The wind derection above the planetary boundary layer seems to have the constant value of about 240°. However, on a weather map it is found that further south (west of Bergen, B) the wind is more from the south. It is therefore guessed that the direction at Stad is as indicated by the arrow on fig. 5.2. Except for a thin, very stable layer near the ground, the Scorer parameter $\gamma=N/U$ has an almost constant value of 0.7-0.8 up to 620 mb (=3.7 km) where it drops to about 0.2. Thus the atmospheric situation is well approximated by the two-layer model we use in this paper.

To make a choice we take $\gamma_1=0.8$, $\gamma_2=0.2$, $h=3.7$. The relative humidity is 98% at 700 mb, and less than this at all other levels. Thus it is reasonable to assume that the clouds making the lee-waves visible are situated at this level, and we compute the wave field at $z=h=3.7$.

The "corner" at Stad is approximated by (4.3) with $\alpha(x)=-\frac{1}{2}|x|$. The corner angle is then 127°, which agrees quite well with the angle measured on the map. Anyhow we do not expect that the choice of this angle is crucial since earlier computations of lee-waves behind isolated obstacles (Marthinsen (1980)) have shown that the shape of the mountain does not influence the wave field very much.

Fig. 5.4 shows a part of the wave pattern. Only the positive values of η, corresponding to the visible clouds, are displayed. The corner is situated at $x=y=0$, and the solid line is the "coast", $y=-\frac{1}{2}|x|$, with land below. If we measure the wavelength on the photograph, we find that it is about 12 km, and measuring at fig. 5.4 gives 12.1 km, so there is good agreement. The wavelength, however, is determined exclusively by the atmospheric conditions, so that the good agreement here has nothing to do with how the waves are generated.

Let us instead try to compare the shape of the computed wave-crests with those observed. Since we have only computed the pole-contribution to η, the computation is only valid some distance from land. Thus we do not look at the lower left corner of fig. 5.4. When this part is excluded, however, we see that the shape of the computed waves agrees quite well with the first 5-6 wave crests on the photograph. Further north the crests bend more northwards, and the wavelength decreases. This is most probably due to a horizontal variation in wind direction and speed. Such effects are not included in the model considered here.

The waves on the photograph differ from waves generated by an isolated peak in that they curve away from the y-axis. Fig. 5.5 shows the lee-waves behind a single peak with the same atmospheric conditions. The waves there curve towards the y-axis, while for the waves generated by a corner (fig. 5.4), the curvature has the correct direction.

Accepting now that the waves in this case are generated by a relatively large scale structure where the individual peaks are wiped out, there still remains an open question. Why is it that sometimes the situation is as it is here, while at other times the individual peaks generate their own separate waves, and a quite irregular interference pattern is observed? This question we do not attempt to answer here.

As mentioned in section 3 the waves behind an obstacle consist of transverse waves with crests nearly perpendicular to the wind and diverging waves inclined to the wind (like the Kelvin ship wave pattern) with the transverse waves sometimes partially or completely missing. Only when the transverse waves are fully developed, will there be any lee-waves in a two-dimensional flow behind a long mountain ridge. In order for this to be the case there must exist a solution to (2.19) with $l=0$, that is

$$D(k_o,0) = 0 \tag{5.1}$$

where

$$D(k,0) = \sqrt{\gamma_1^2-k^2}\cos(\sqrt{\gamma_1^2-k^2}\,h) + \sqrt{k^2-\gamma_2^2}\sin(\sqrt{\gamma_1^2-k^2}\,h)$$

Since we must have $\gamma_2 < k_o < \gamma_1$, (5.1) has a solution if

$$\frac{D(k_1,0)}{\sqrt{\gamma_1^2-k^2}} \quad \frac{D(k_2,0)}{\sqrt{\gamma_1^2-k^2}} < 0$$

that is

$$(1+\sqrt{\gamma_1^2-\gamma_2^2})\cos(\sqrt{\gamma_1^2-\gamma_2^2}\,h) < 0$$

Thus a sufficient condition for the transverse waves to be fully developed is that

$$\gamma_1^2 - \gamma_2^2 > \frac{\pi^2}{4h^2} \tag{5.2}$$

One can also show that this is a necessary condition. The criterion was first derived by Scorer (1949).

In cases when (5.2) is not satisfied, something interesting happens at the end of a long ridge. Fig. 5.6 shows the lee-wave pattern behind a circular mountain. The parameter values are $\gamma_1=1.4$, $\gamma_2=0.5$, $h=z=1.2$ so that (5.2) is not satisfied. If we superpose solutions to obtain the lee-wave pattern behind a ridge, eq. (4.1), we find the waves shown on fig. 5.7. The most striking feature here is a 180° phase shift at $y=0$. It seems like $\eta(x,y)=-\eta(x,-y)$ exactly. This can be explained physically. Every point along the ridge acts as a source for a lee-wave pattern as on fig.5.6. This wave pattern is contained in a wedge, with a wedge angle ϕ. Accordingly, at each point downstream of the ridge, the displacement is caused by disturbances inside the wedge angle ϕ upstream of this point, see fig. 5.8. Thus η at P_1 is coused only by the part of the ridge from C to D, while at P_2 it is caused by the segment from C to E. However, since there are in this case no two-dimensional waves behined an infinite ridge, the displacement at P_2 would have been zero if the ridge filled up the whole segment from B to E. Therefore, at P_2 η must have exactly the negative value of what would have been caused by disturbances from B to C, and that is precisely the negative of η at P_1.

6 - Concluding remarks

For an atmosphere with constant γ, the flow past an isolated obstacle changes qualitatively with the parameter γH_o. For the two extremes, γH_o very small and very large, there exists nonlinear solutions of the problem given by Drazin (1961). When γH_o is

small, the linear theory used in the present paper also gives a good approximation. The hydrostatic computations done by Smith (1980) require that γp is large (p is the horizontal length-scale of the obstacle). Thus when γ is small and p has a moderate value, the hydrostatic assumption cannot be made. In section 3 we showed that when $\gamma p=0.2$ the flow was far from hydrostatic; instead it was more like the symmetric flow, while the (near) hydrostatic flow obtained when $\gamma p=1.0$ has strong fore-aft symmetry with lifting in front of and above the mountain and strong sinking in the lee. For large γH_o the nonlinear effects become crucially important, so that the linear hydrostatic theory requires $H_o/p \ll 1$.

The hydrostatic approximation is of limited interest when γ varies with height, since it would neglect important contributions to the dependent quantities. In section 3 we studied the flow past an isolated obstacle for different vertical distributions of γ. It was found among other things that the cross-section of the flow influenced by the mountain increased with increasing difference in γ between the two layers.

In section 5 we looked at trapped lee-waves only and demonstrated that the regular lee-wave pattern along the norwegian coast seen on fig. 5.1 could very well be generated by a relatively large scale topographic structure where the individual peaks are smoothed out. We are not, however, able to explain why the peaks are smoothed out in some cases but not in others.

REFERENCES

Blumen, W. and McGregor, C.D. 1976 Wave drag by three-dimensional mountain lee-waves in nonplanar shear flow. Tellus 28, 287-298

Crapper, G.D. 1959 A three-dimensional solution for waves in the lee of mountains. J.Fluid Mech. 6, 51-76

Crapper, G.D. 1962 Waves in the lee of mountains with elliptical contours. Phil.Trans.Roy.Soc., London (A) 254, 601-623

Drazin, P.G. 1961 On the steady flow of a fluid of variable density past an obstacle. Tellus 13, 239-251

Gjevik, B. 1980 Orographic effects revealed by satellite pictures. GARP publication series No 23. WMO

Gjevik, B. and Marthinsen, T. 1978 Three-dimensional lee-wave pattern. Quart.J.R.Met.Soc. 104, 947-957

Marthinsen, T. 1980 Three-dimensional lee-waves. Quart.J.R.Met. Soc. 106, 569-580

Mobbs, S.D. 1981 Lecture given at the eighth meeting of the European Geophysical Society, 24-29 august 1981

Palm, E. 1958 Two-dimensional and three-dimensional mountain waves. Geof.Publ. (Oslo) 20, No 3, 1-25.

Sawyer, J.S. 1962 Gravity waves in the atmosphere as a three-dimensional problem. Quart.J.R.Met.Soc. 88, 412-425

Scorer, R.S. 1949 Theory of lee-waves of mountains. Quart.J.R.Met. Soc. 75, 41-56

Scorer, R.S. 1956 Airflow over an isolated hill. Quart.J.R.Met.Soc. 82, 75-81

Scorer, R.S. and Wilkinson, M. 1956 Waves in the lee of an isolated hill. Quart.J.R.Met.Soc. 82, 419-427

Smith, R.B. 1980 Linear theory of stratified hydrostatic flow past an isolated mountain. Tellus 32, 348-364

Wurtele, M. 1957 The three-dimensional lee-wave. Beitr.Phys.frei. Atmos. 29, 242-252

Figure captions

Fig 2.1 The atmospheric model. $\gamma=N/U$, the Scorer parameter.

Fig. 2.2 Path of integration. The path is taken below the singularities so that these only contribute for $x>0$.

Fig. 3.1-3.20 Lines of constant η. Solid lines lifting or zero, broken lines sinking. The values of η are $\eta=\pm 0.05H_o$, $\pm 0.1H_o$,... . The parameter values for the figures are shown in the table below

Fig.	γ_1	γ_2	h	z
1	0.2	0.2	1.0	1.0
2	1.0	1.0	1.0	1.0
3	0.2	0.2	2.0	2.0
4	0.4	0.2	1.0	1.0
5	0.6	"	"	"
6	0.8	"	"	"
7	1.0	"	"	"
8	"	0.0	"	"
9	"	0.4	"	"
10	"	0.6	"	"
11	"	0.8	"	"
12	"	0.2	"	"
13	"	"	1.5	"
14	"	"	2.0	"
15	"	"	2.5	"
16	"	"	3.0	"
17	"	"	6.0	"
18	"	"	2.0	0.5
19	"	"	"	1.5
20	"	"	"	2.0

Fig. 3.21 η as a function of x for $z=0.0,0.05,\ldots,1.0$ when $y=0$, $H_o=1.0$, $\gamma_1=\gamma_2=1.0$ in 3.21a and $\gamma_1=\gamma_2=0.2$ in 3.21b. The thick, broken line is the ground.

Fig. 3.22 As fig. 3.21, but $H_o=0.5$.

Fig. 4.2 η-contours for the flow past a ridge given by eq. (4.4). The thick line is the "top" of the ridge, i.e. $\frac{\partial R}{\partial x}=0$, and $R>R_o/2$.

Fig. 5.1 Satellite photograph showing a lee-wave pattern along the western coast of Norway. (Reproduced with the kind permission of Department of Electrical Engineering, University of Dundee).

Fig. 5.2 Map of Norway with the lee-wave crests observed on fig. 5.1 indicated, starting at S. To the left is the "corner" used in the model. The two points S are ment to correspond.

Fig. 5.3 The upper air data as recorded by a radiosonde released at Ørland (Ø on fig. 5.2) one hour after the photograph 5.1 was taken.

Fig. 5.4 η-contours generated by the "corner" on fig. 5.2. Only nonnegative values are shown. $\gamma_1=0.8$, $\gamma_2=0.2$, $z=h=3.7$. The thick line is the "coast".

Fig. 5.5 η-contours generated by an isolated, obstacle with the same atmosphere as on fig. 5.4.

Fig. 5.6 Diverging lee-waves behind a single peak. $\gamma_1=1.4$, $\gamma_2=0.5$, $z=h=1.2$.

Fig. 5.7 Lee-waves behind the end of a long ridge. The ridge is along the positive y-axis. The atmosphere is as on fig. 5.6.

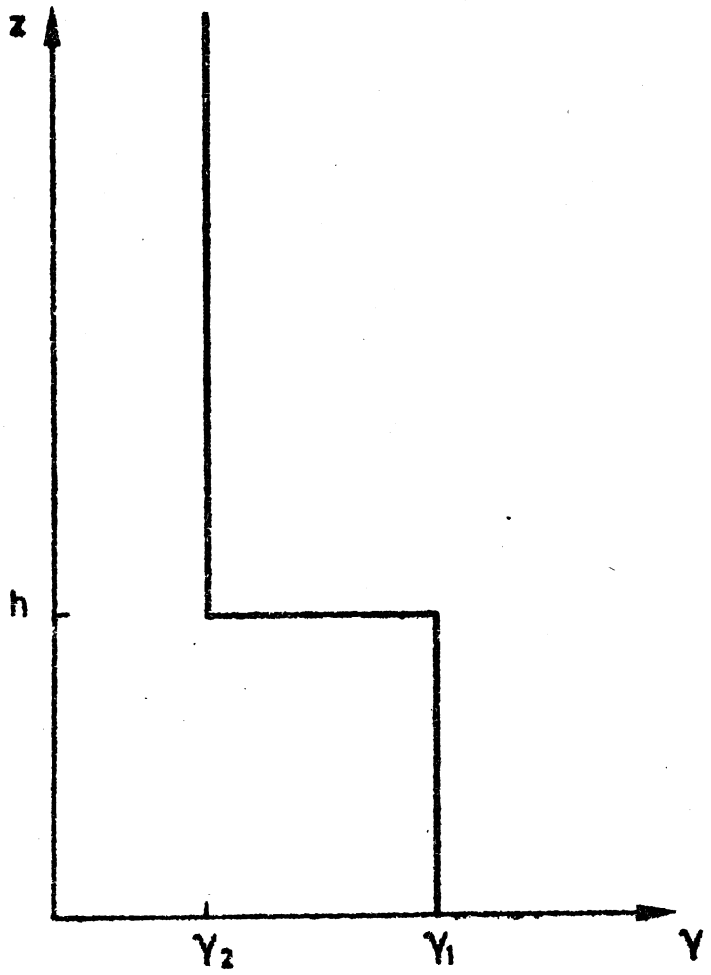

fig. 2.1

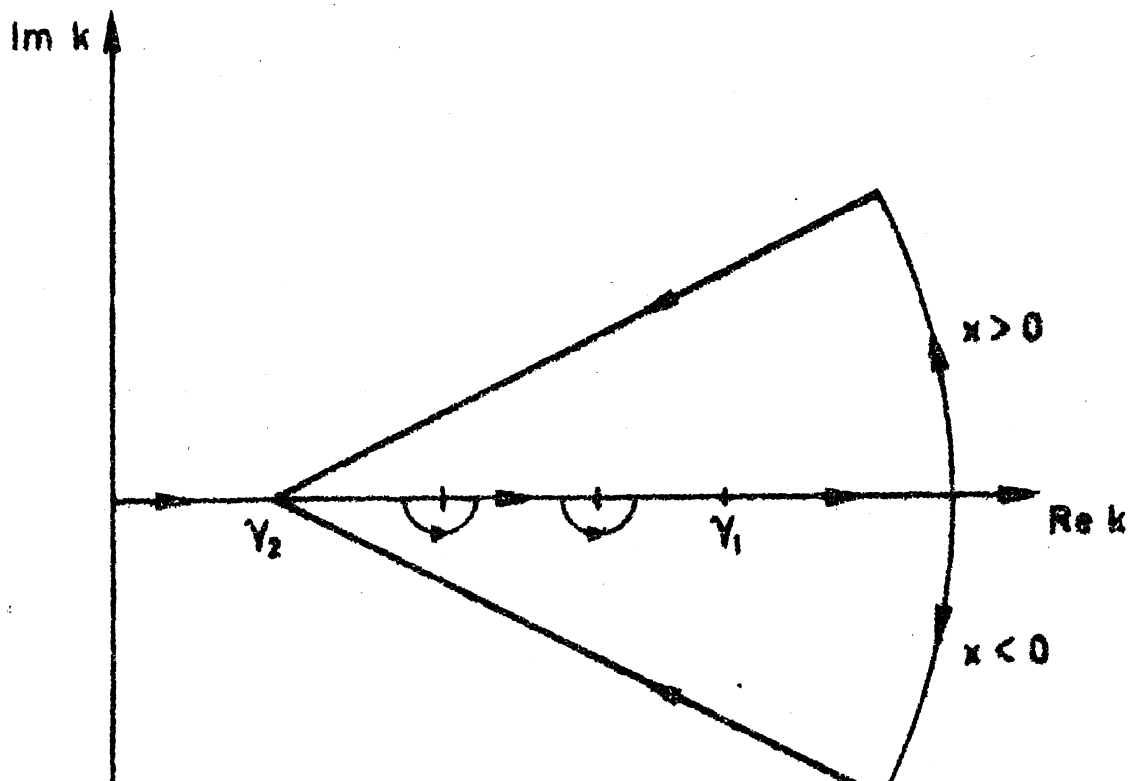

fig. 2.2

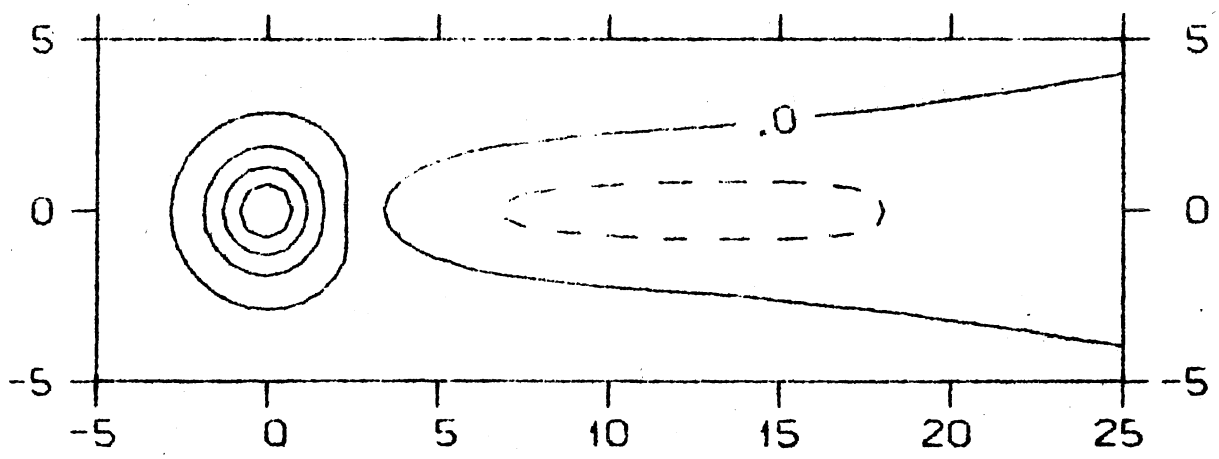

fig. 3.1

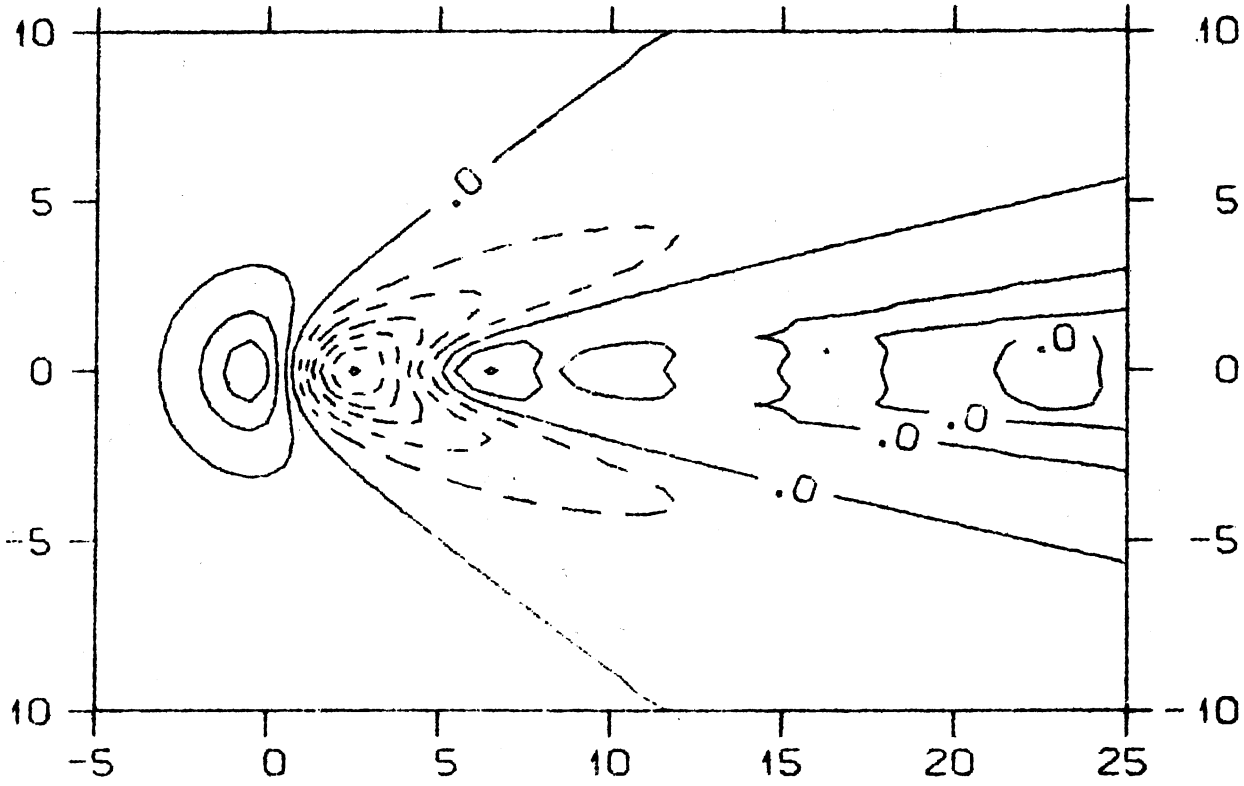

fig. 3.2

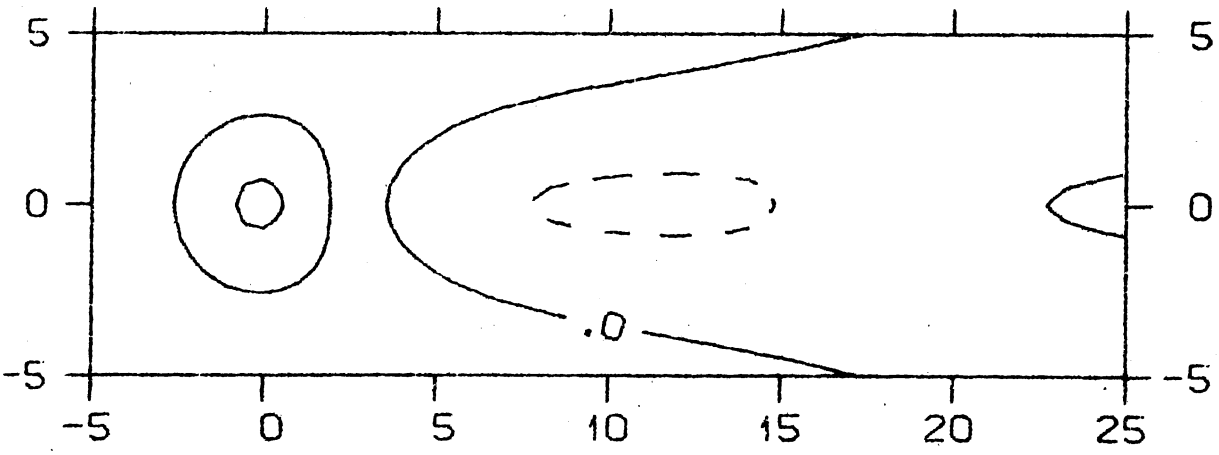

fig. 3.3

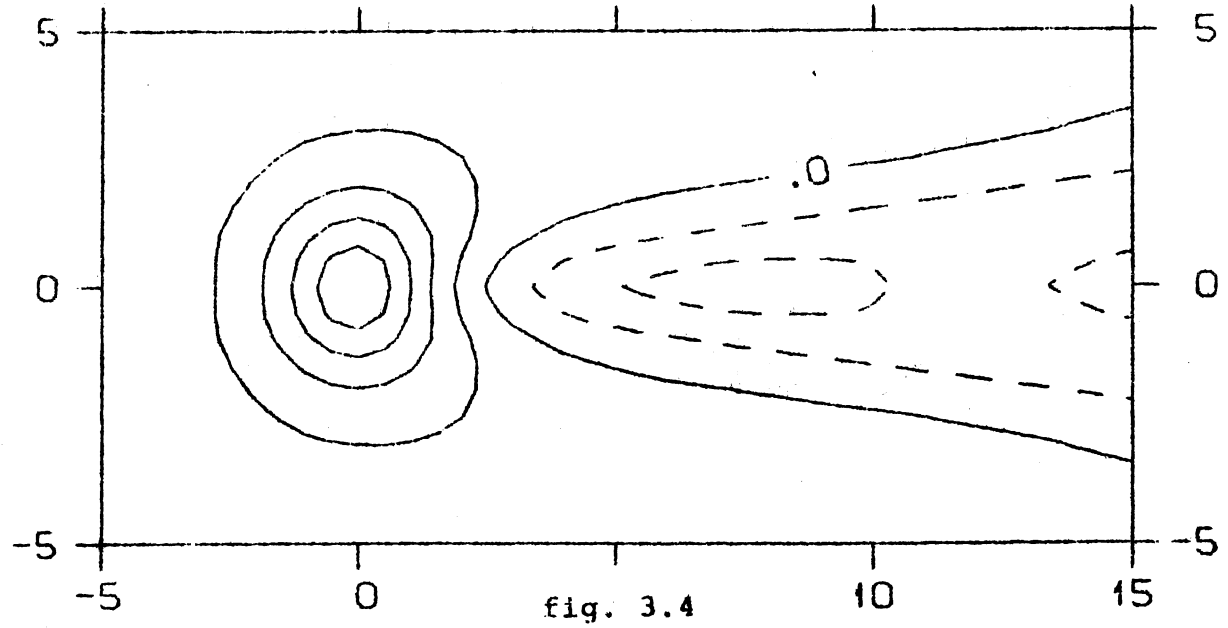

fig. 3.4

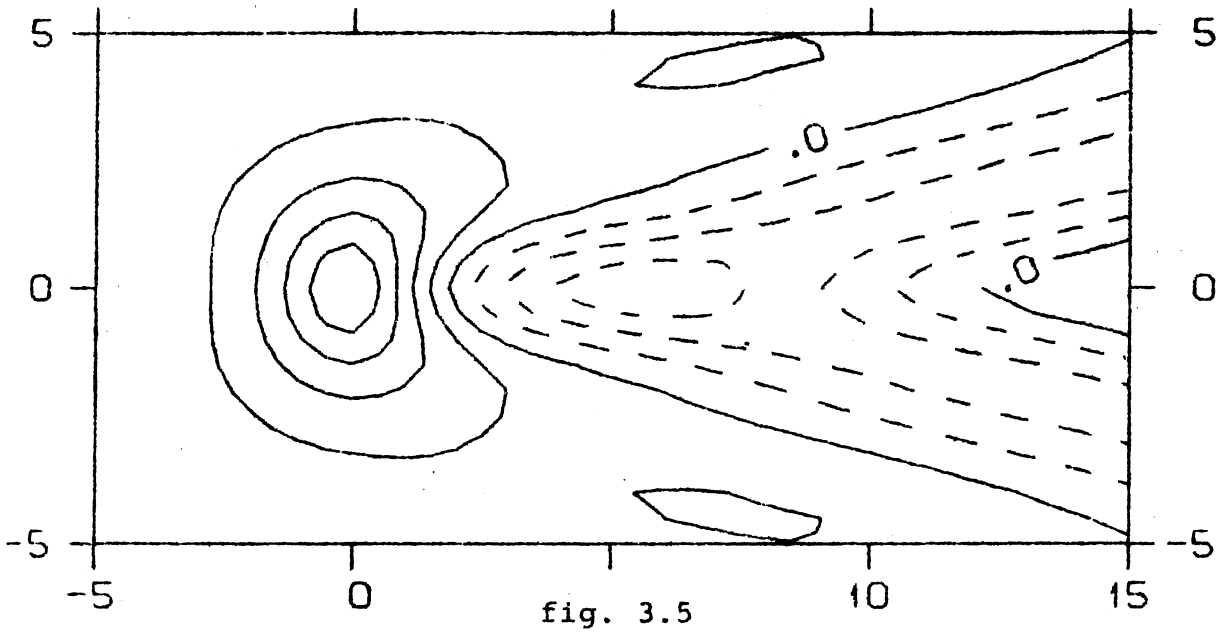

fig. 3.5

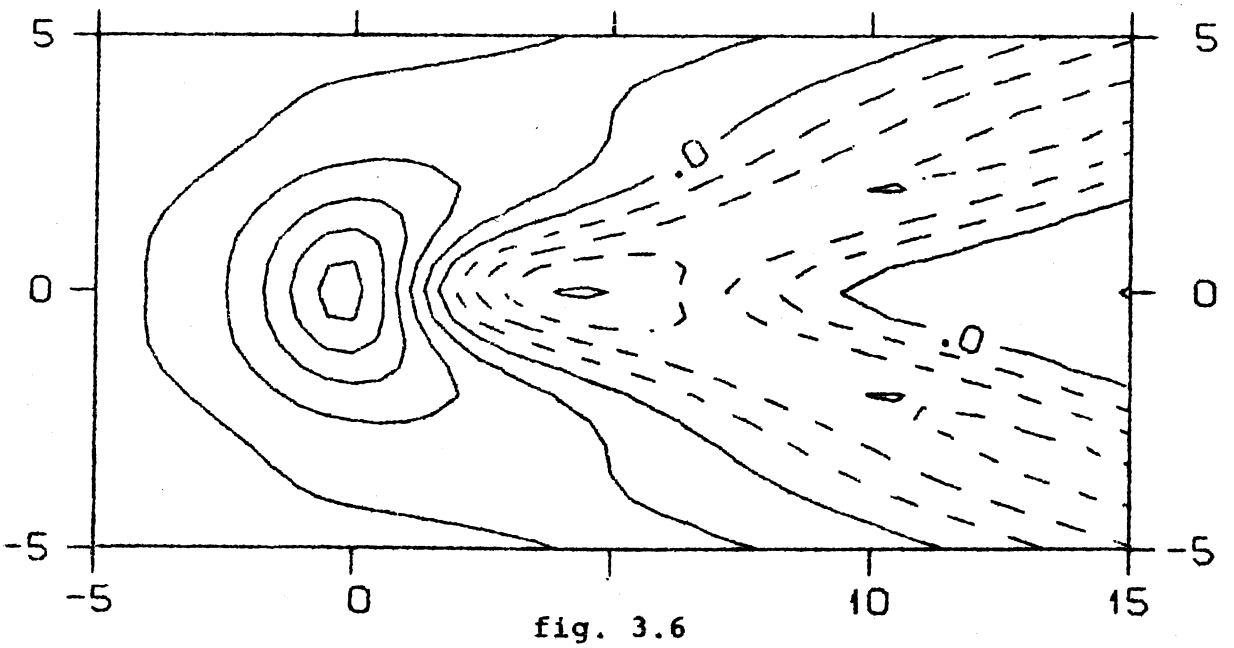

fig. 3.6

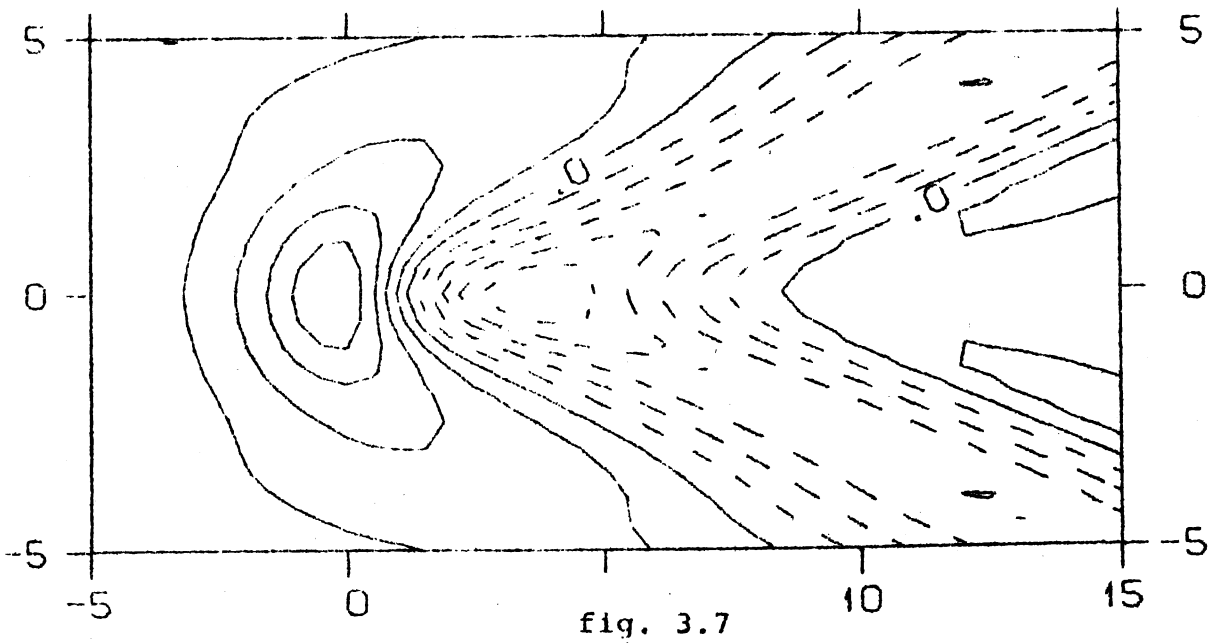

fig. 3.7

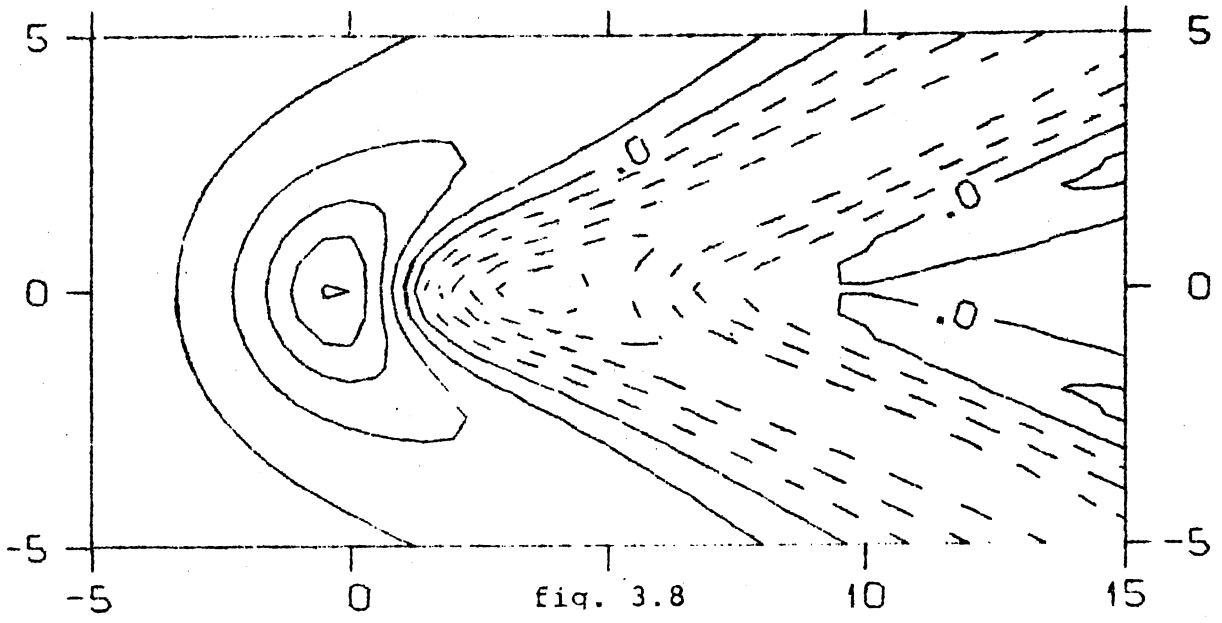

fig. 3.8

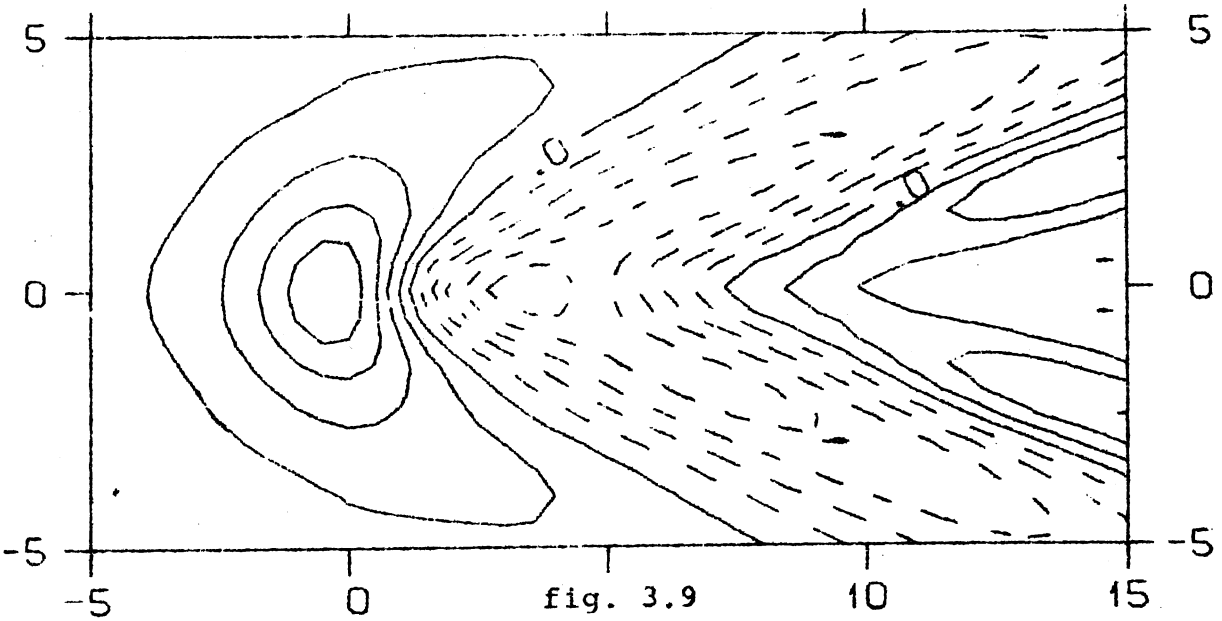

fig. 3.9

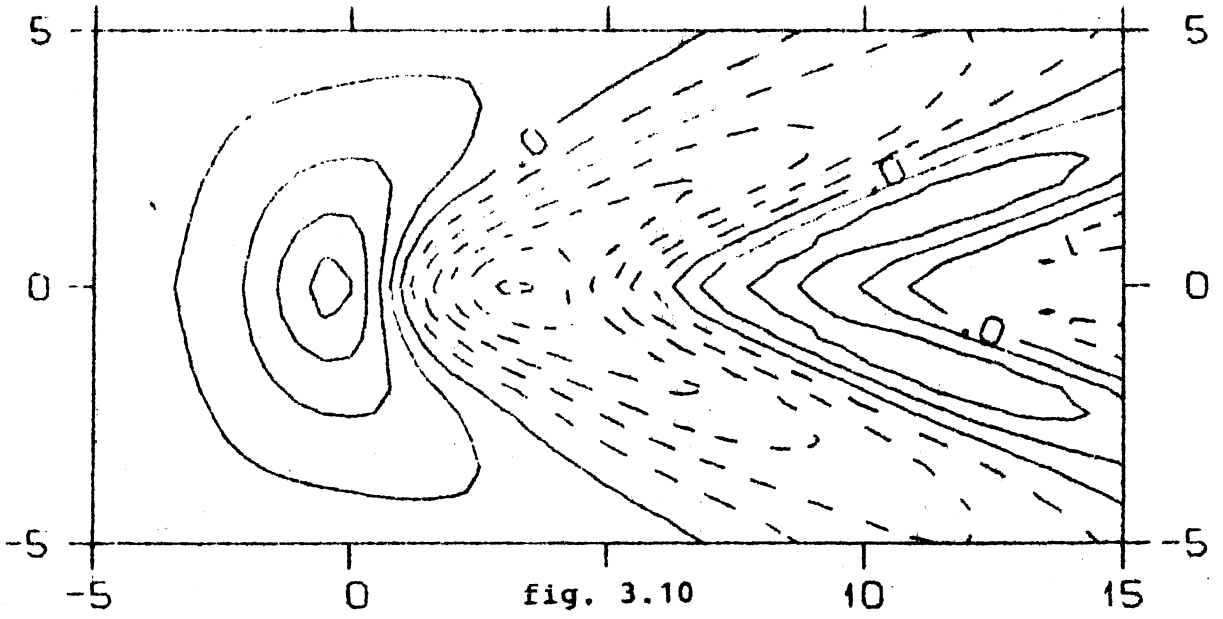

fig. 3.10

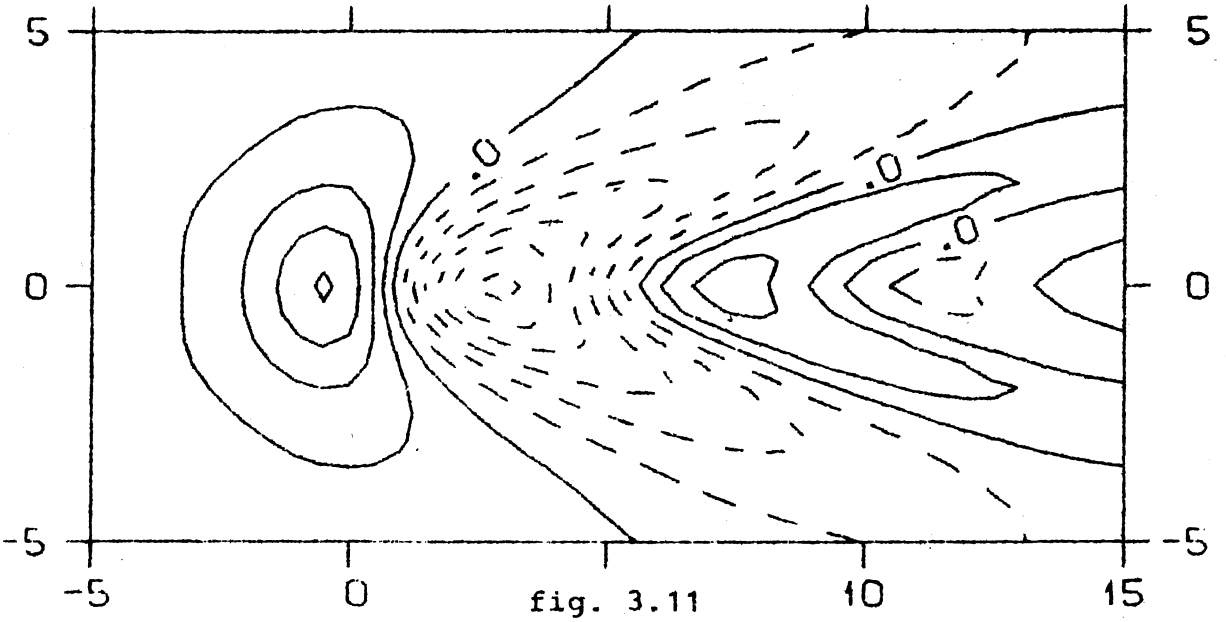

fig. 3.11

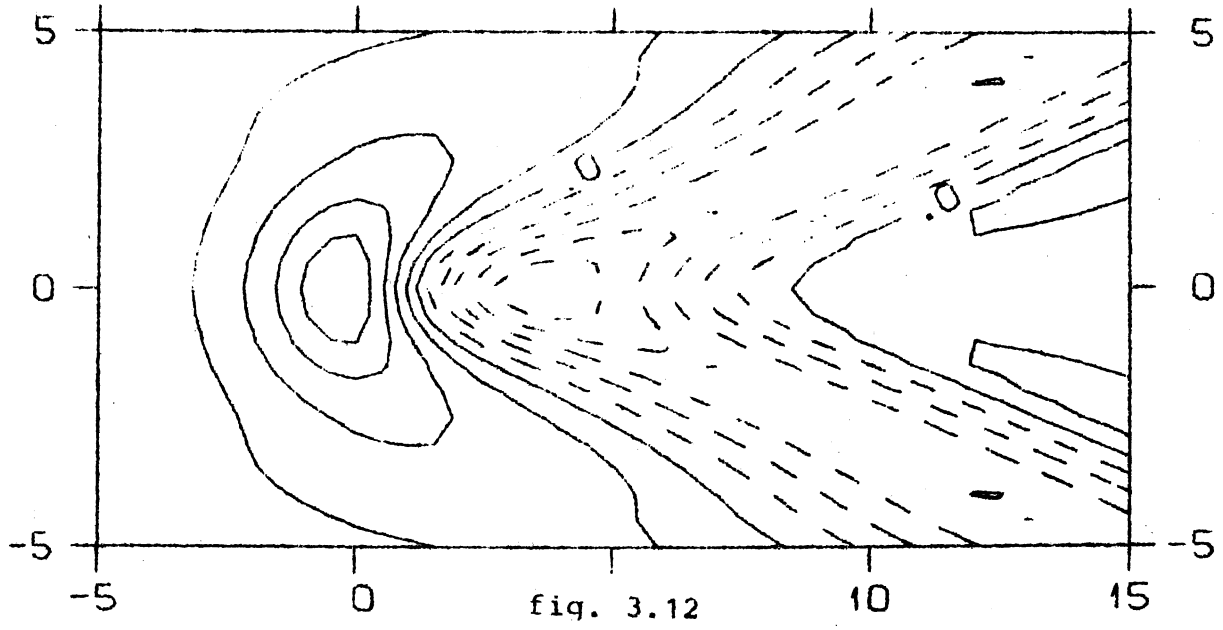

fig. 3.12

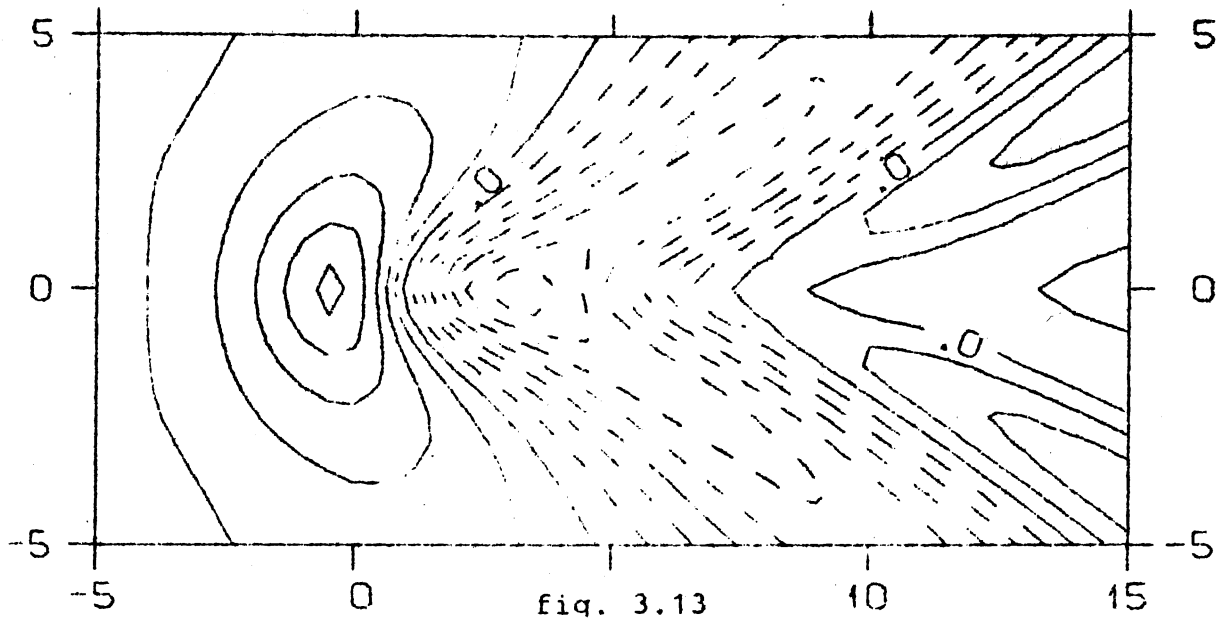

fig. 3.13

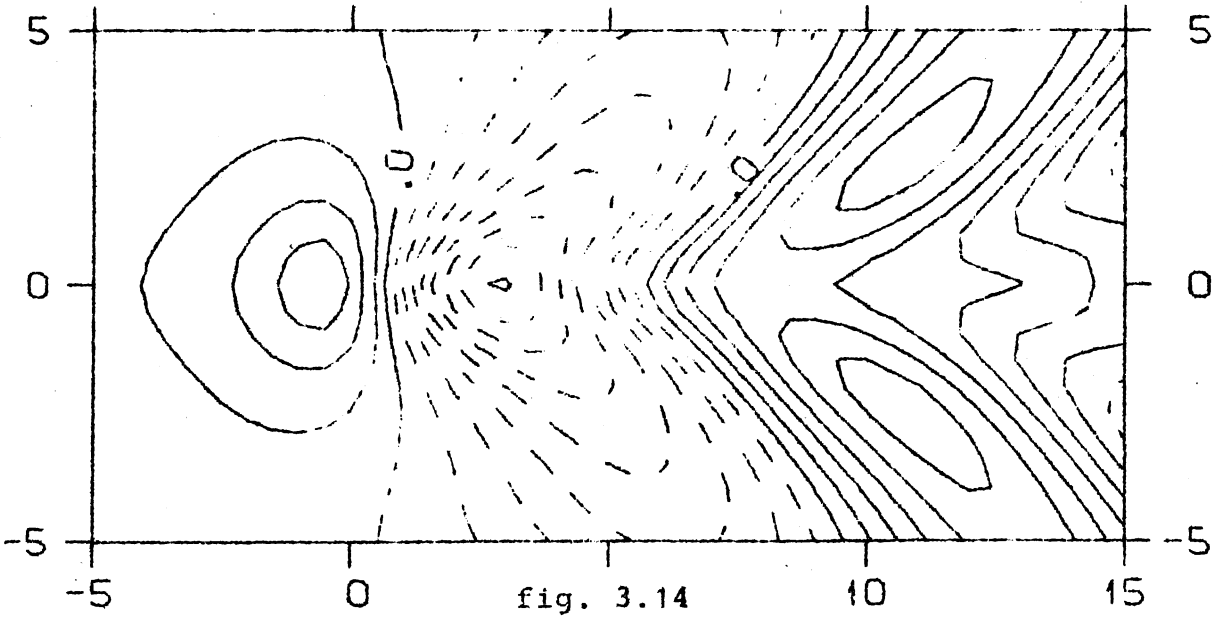

fig. 3.14

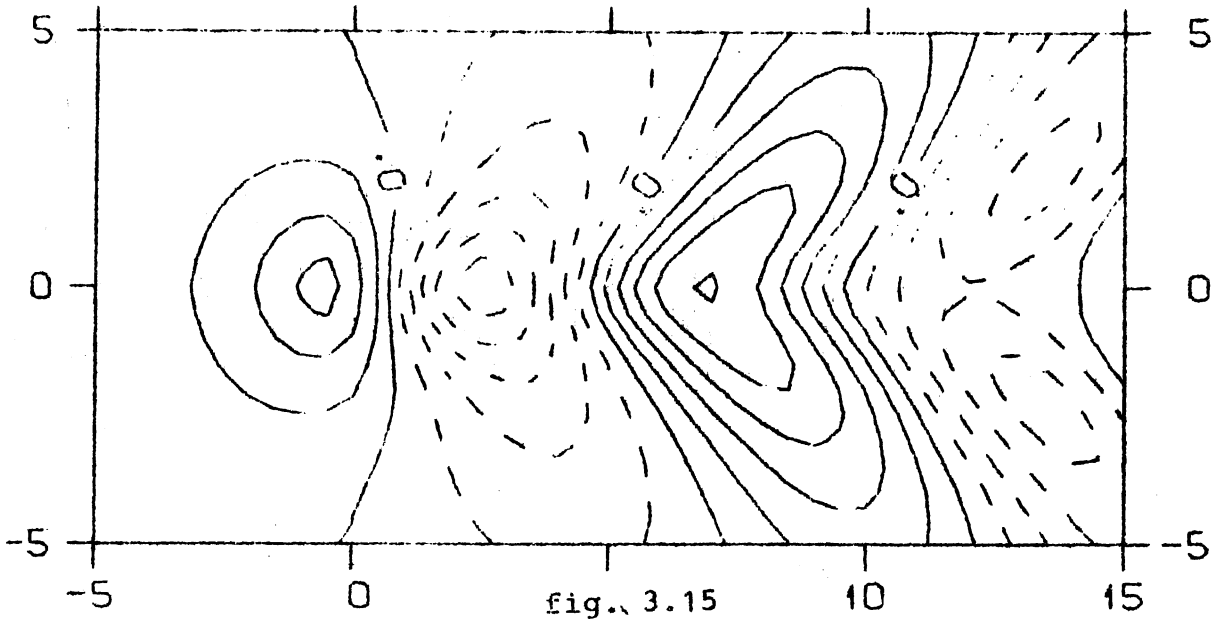

fig. 3.15

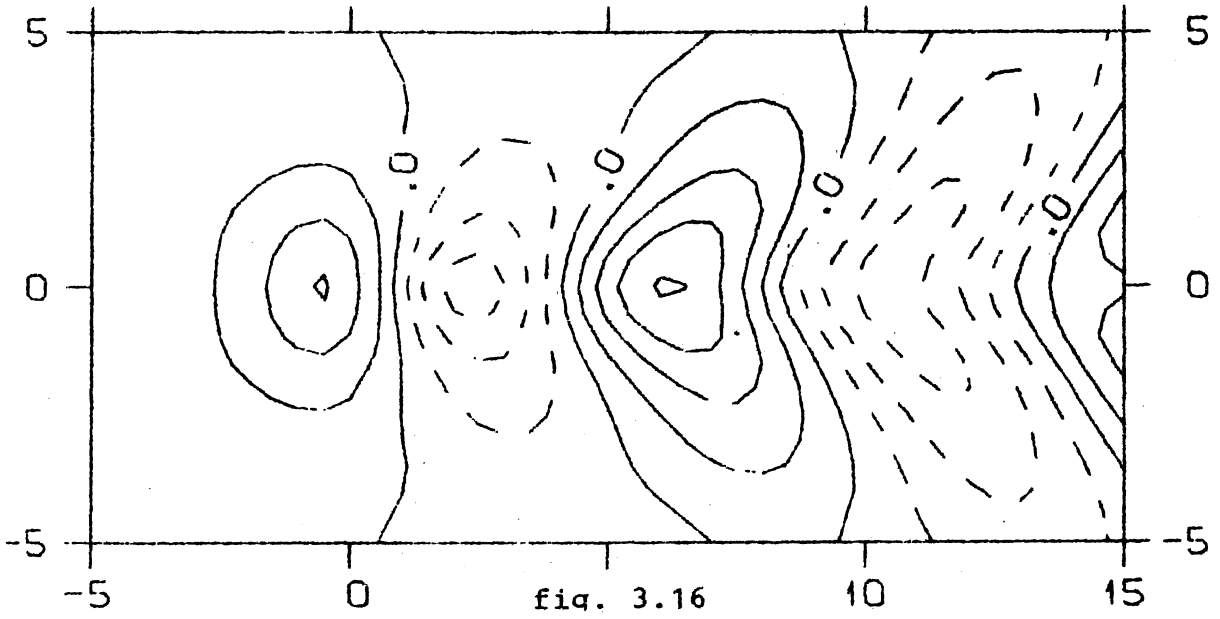

fig. 3.16

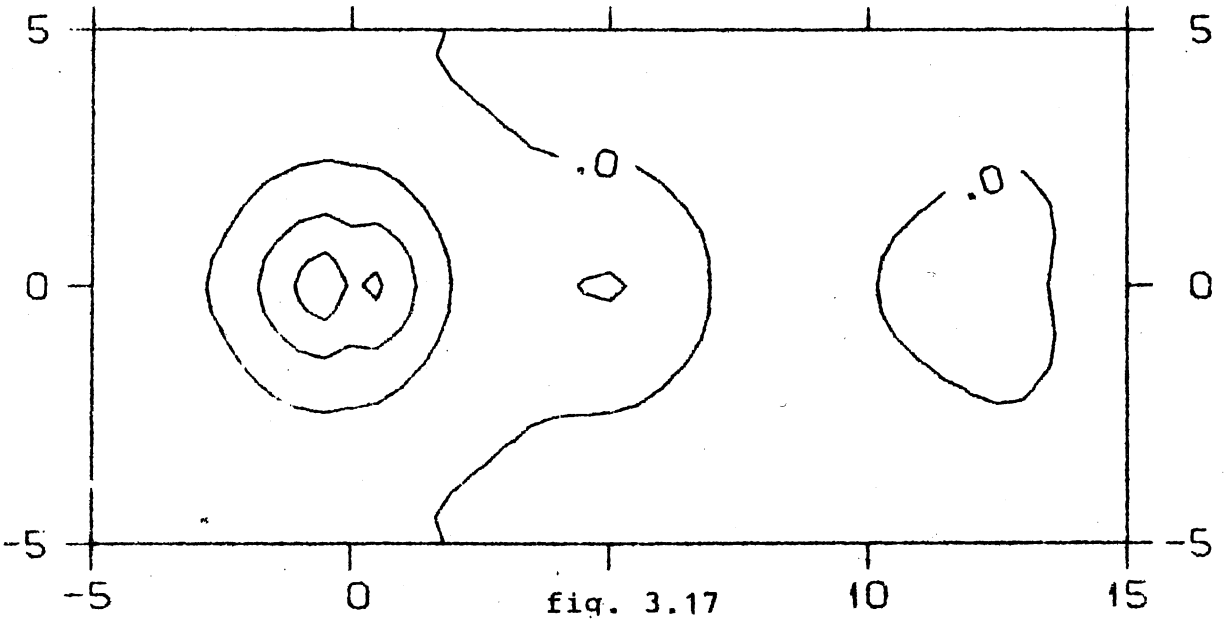

fig. 3.17

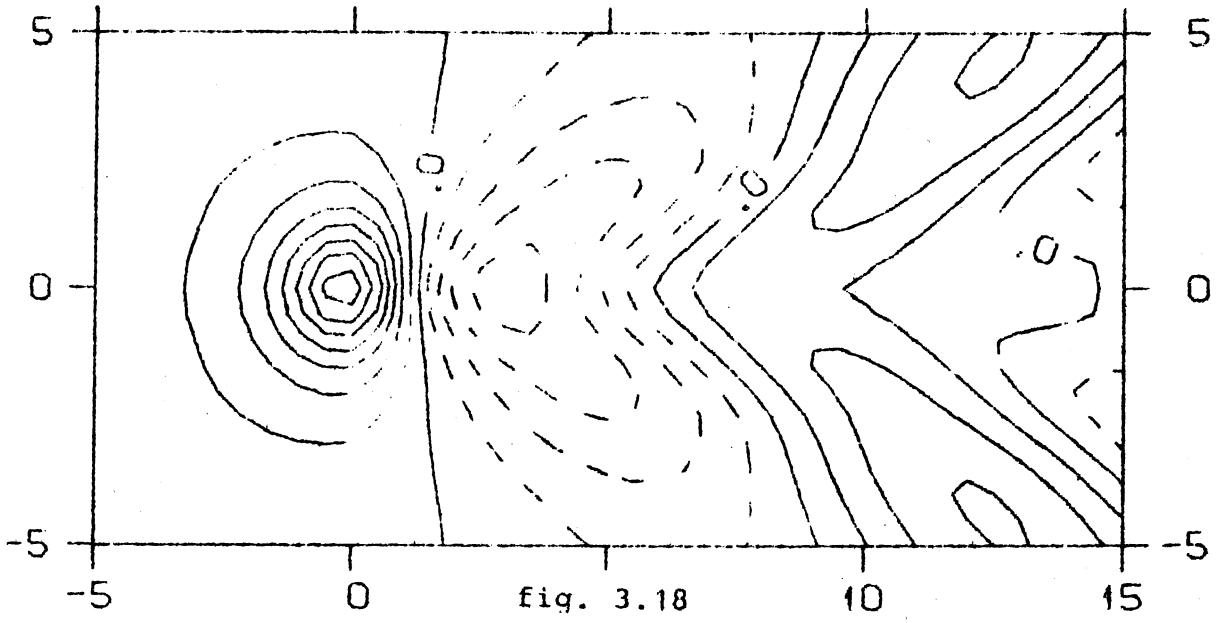

fig. 3.18

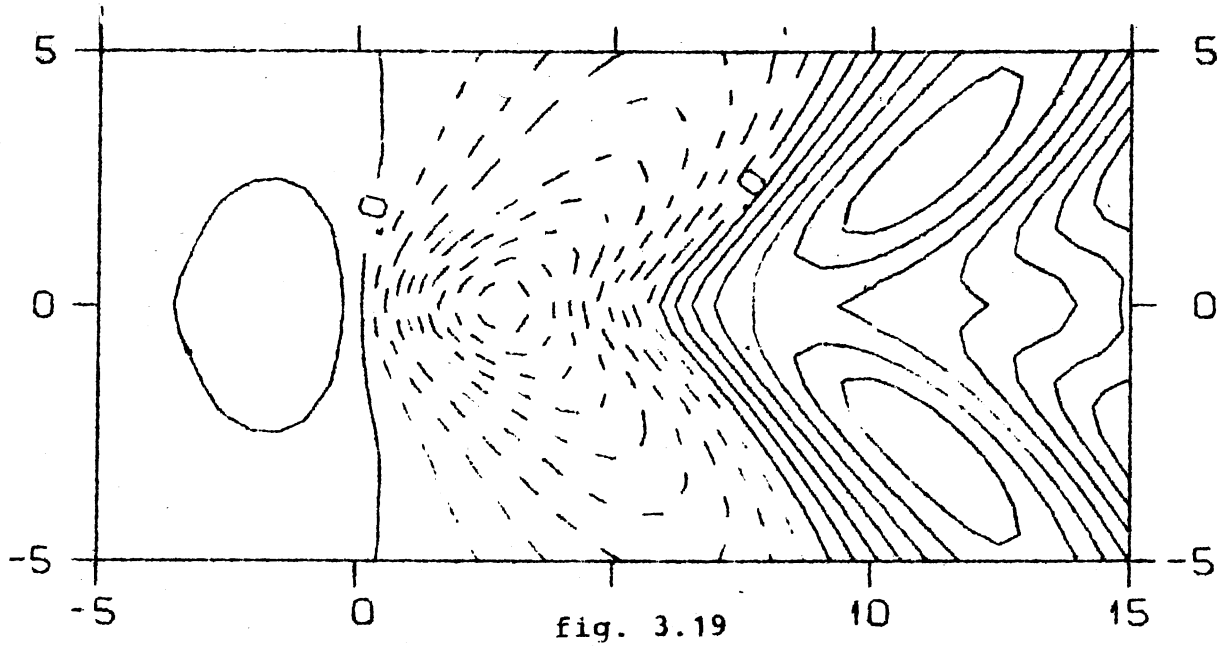

fig. 3.19

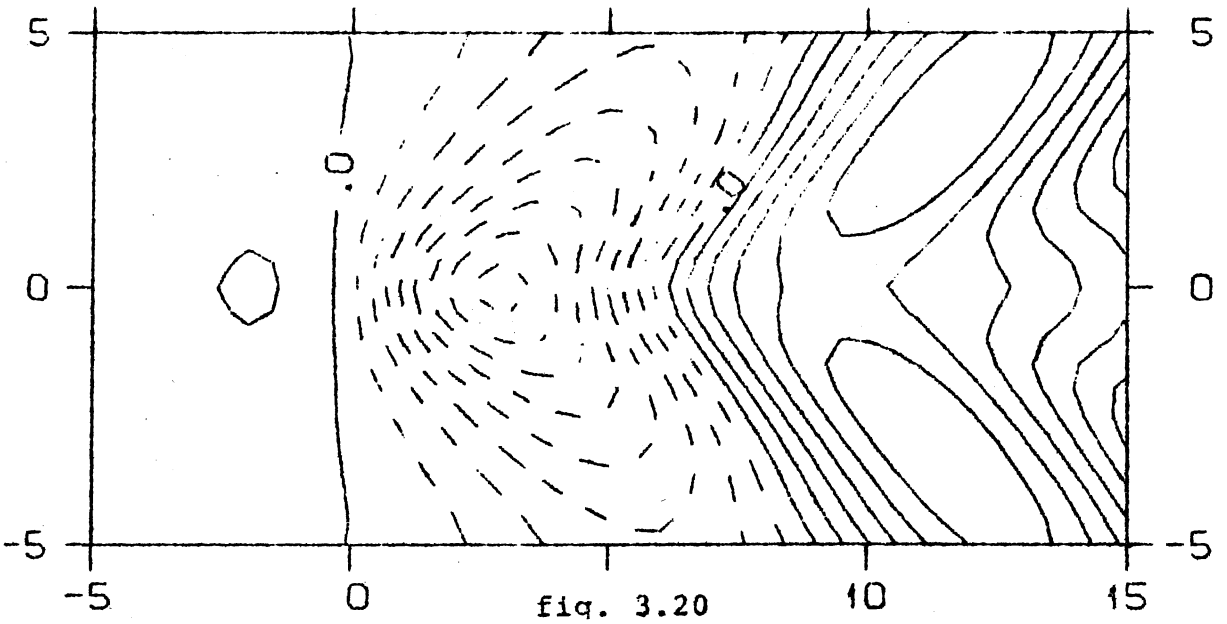

fig. 3.20

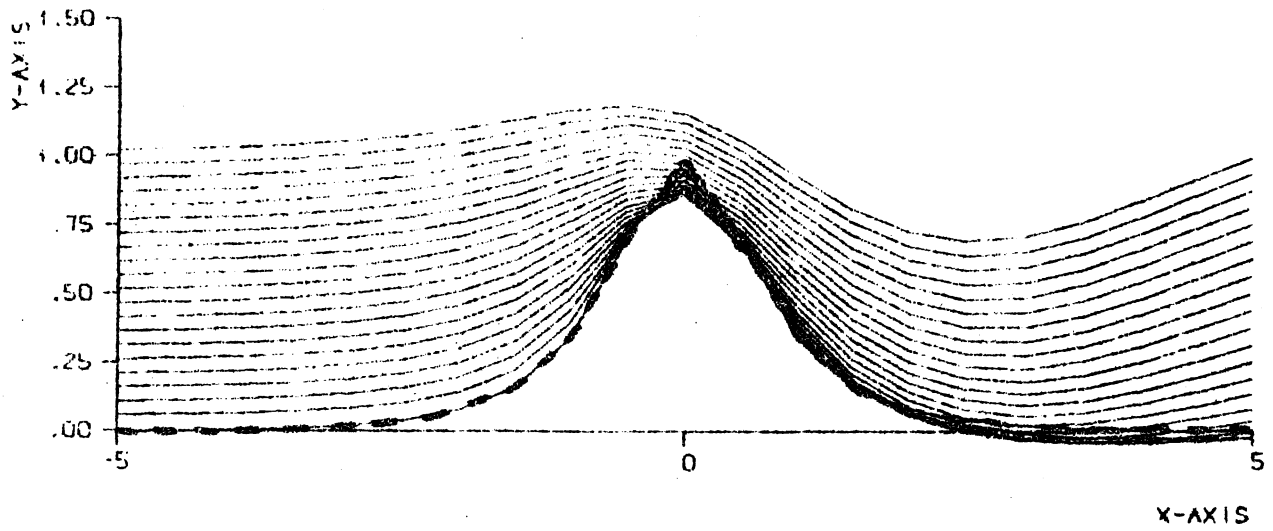

fig. 3.21a

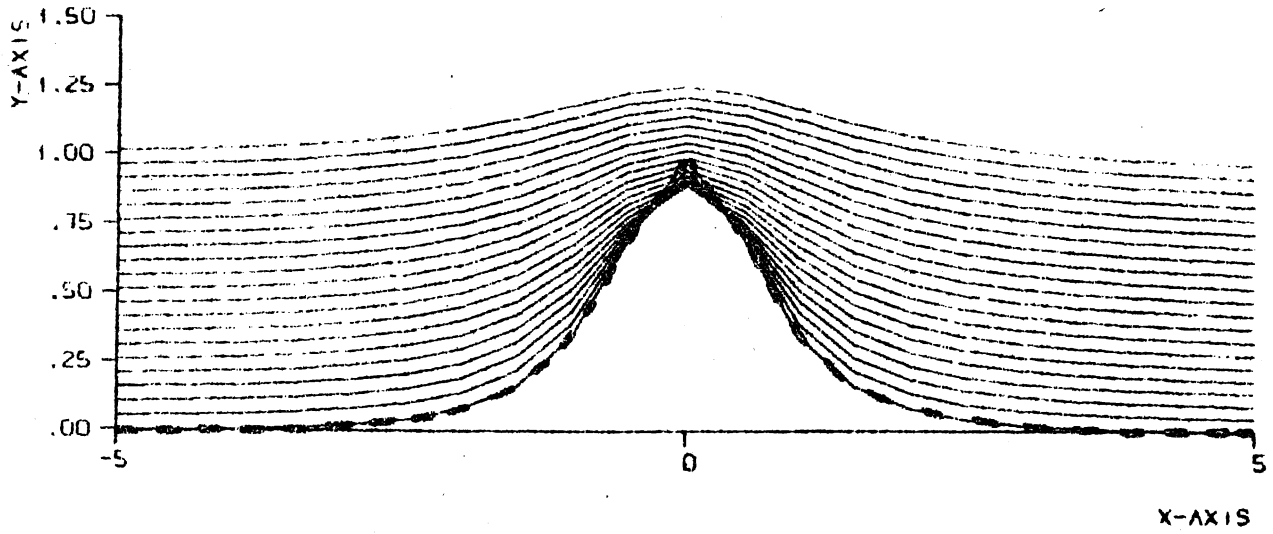

fig. 3.21b

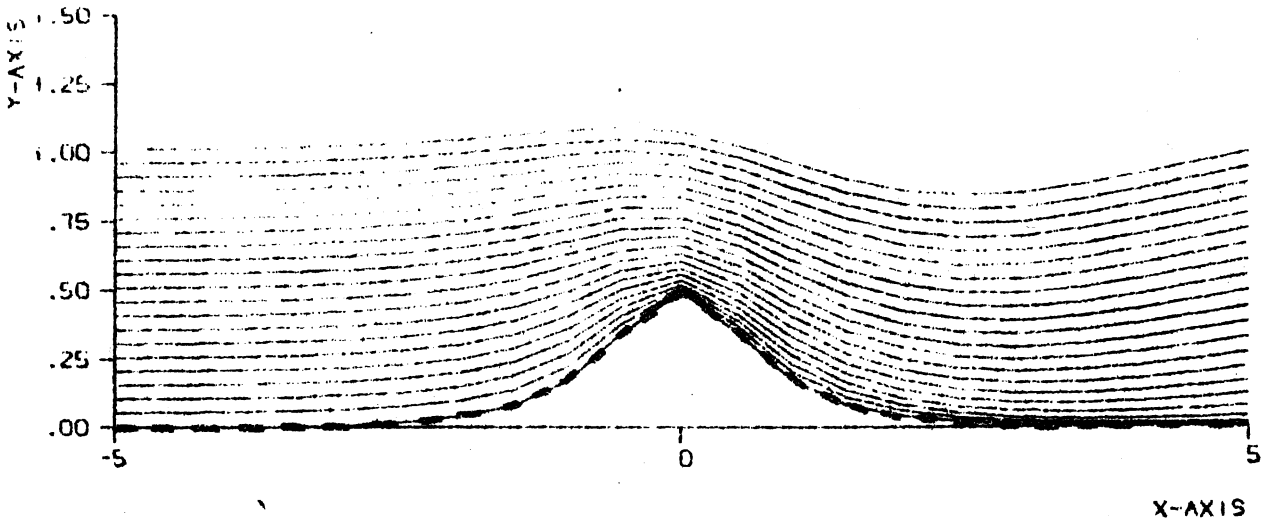

fig. 3.22a

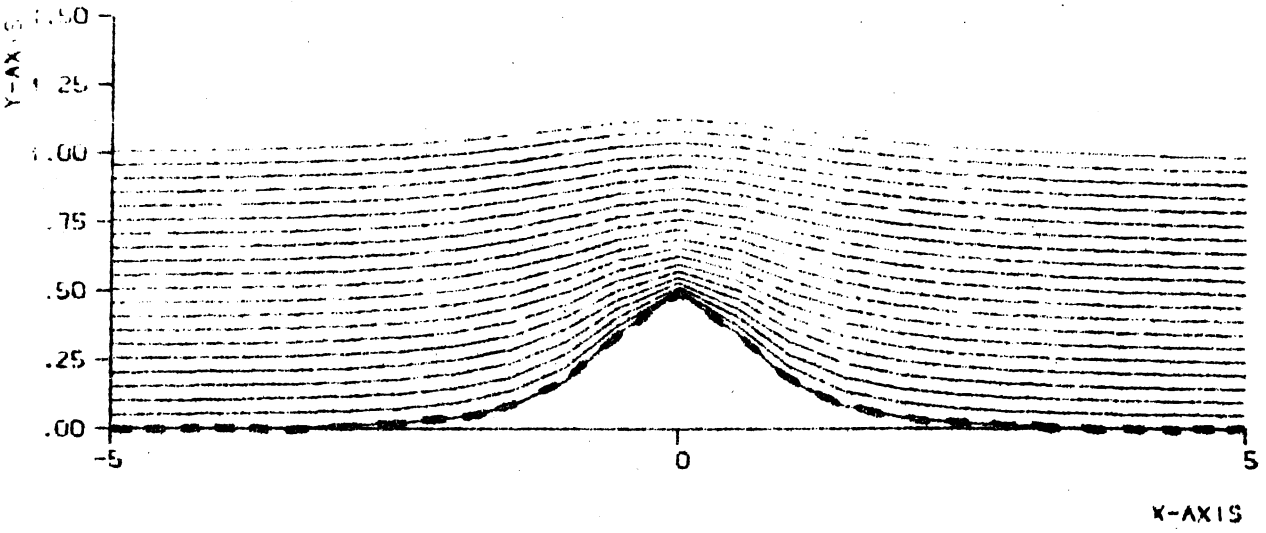

fig. 3.22b

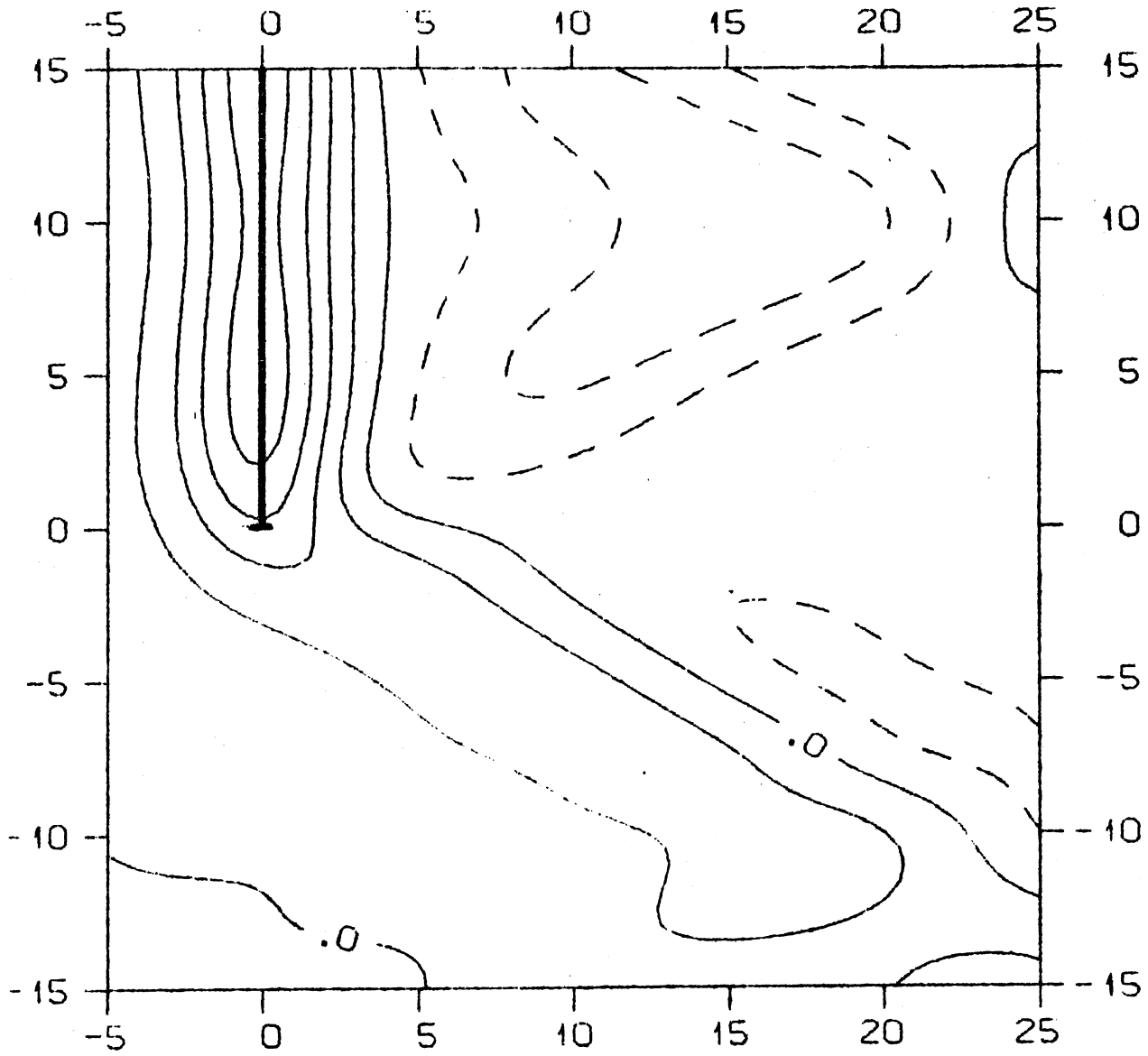

fig. 4.2

fig. 5.1

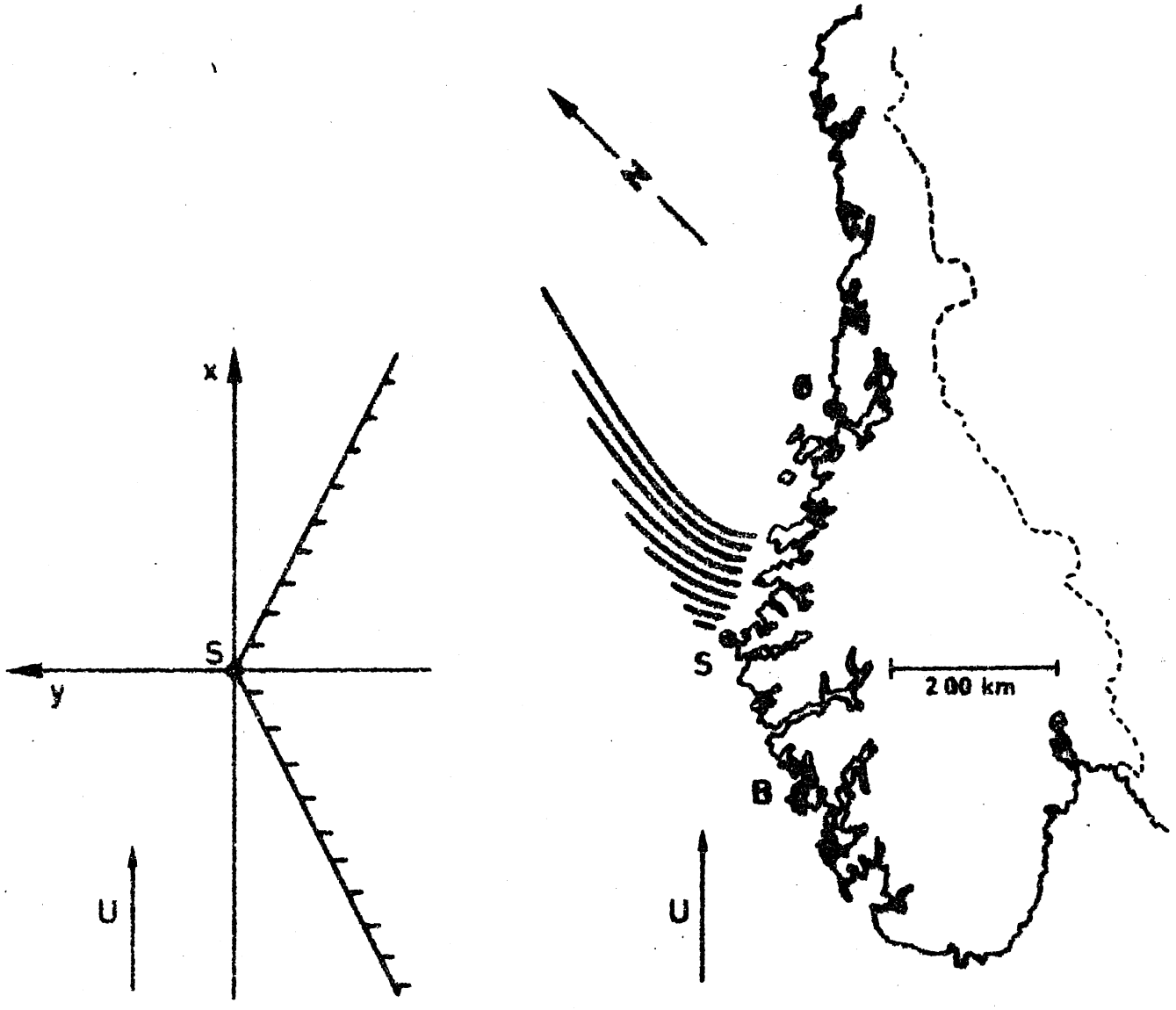

fig.5.2

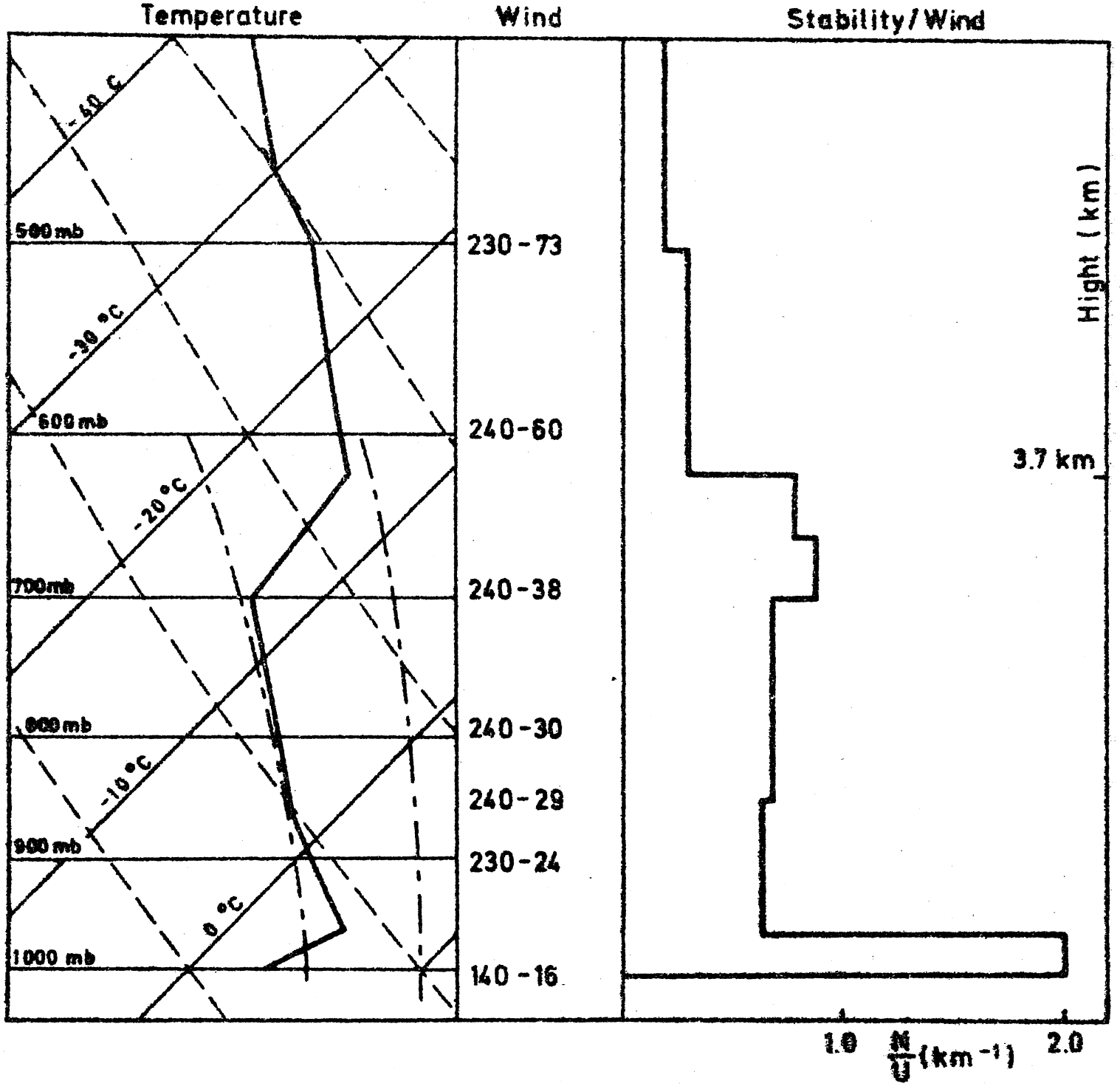
Temperature
Wind
Stability/Wind
-40 C
500 mb
-30 °C
600 mb
-20 °C
700 mb
800 mb
-10 °C
900 mb
0 °C
1000 mb
230 - 73
240 - 60
240 - 38
240 - 30
240 - 29
230 - 24
140 - 16
Hight (km)
3.7 km
1.0
2.0
$\frac{N}{U}$ (km^{-1})

fig. 5.3

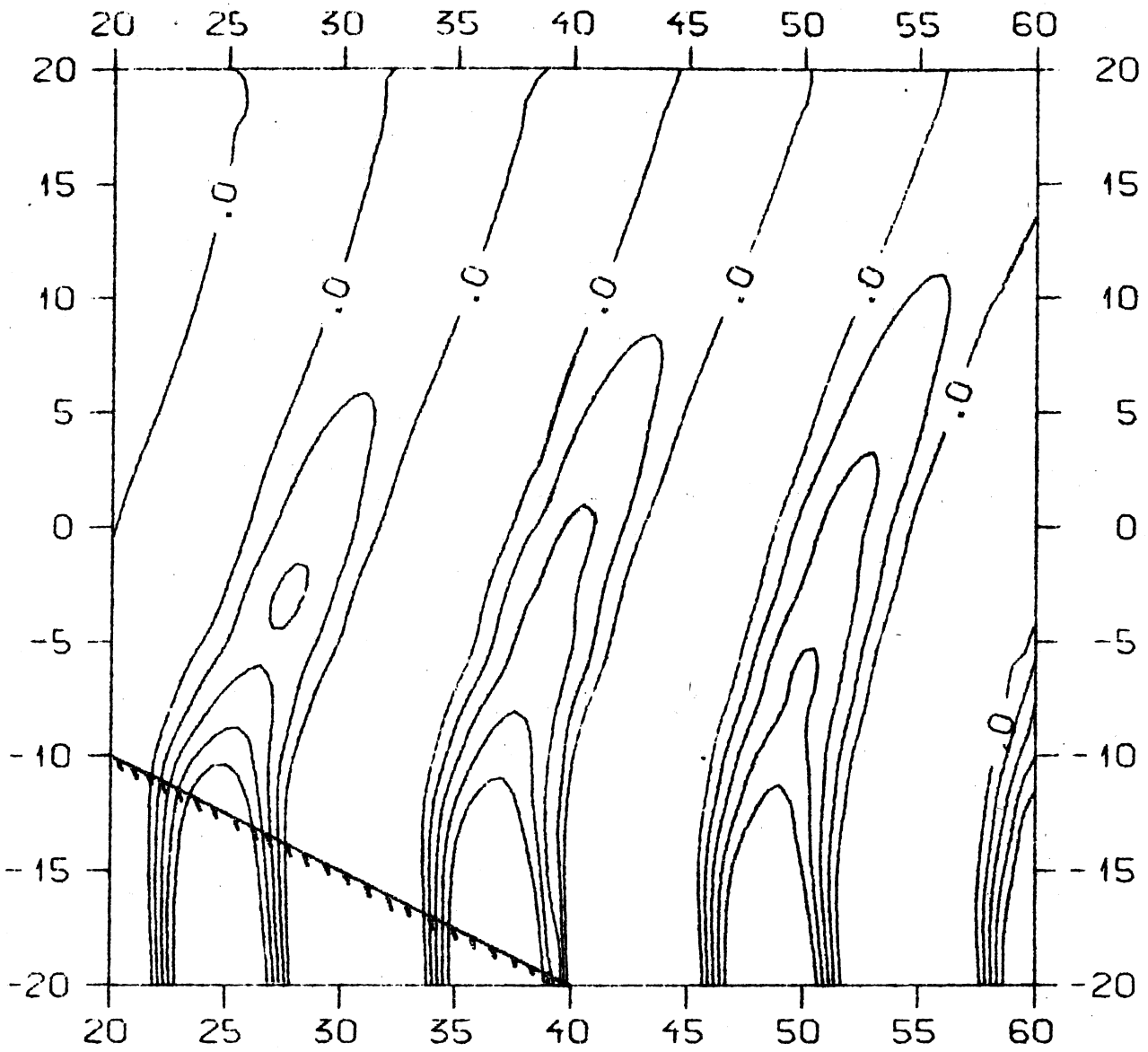

fig. 5.4

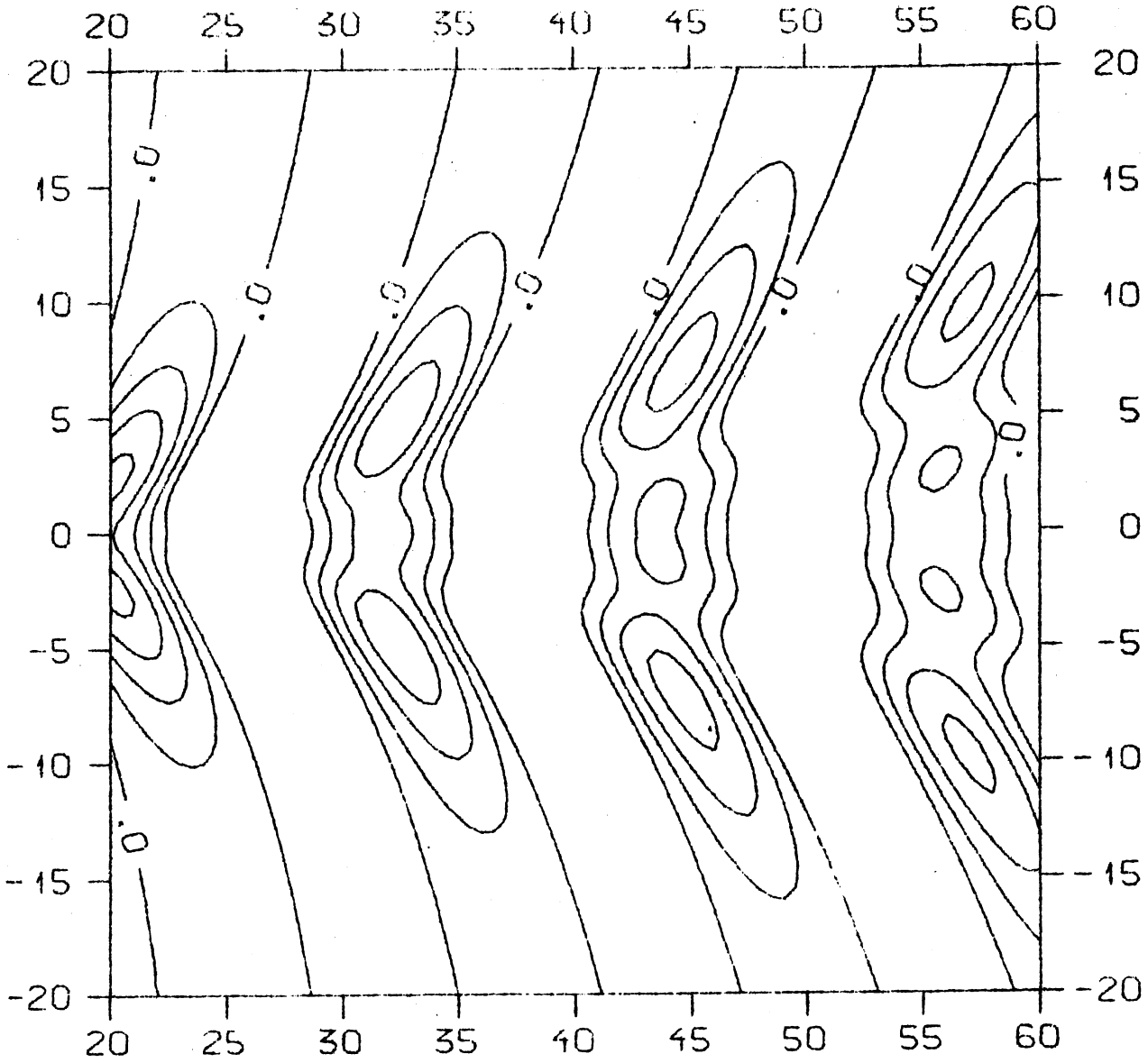

fig. 5.5

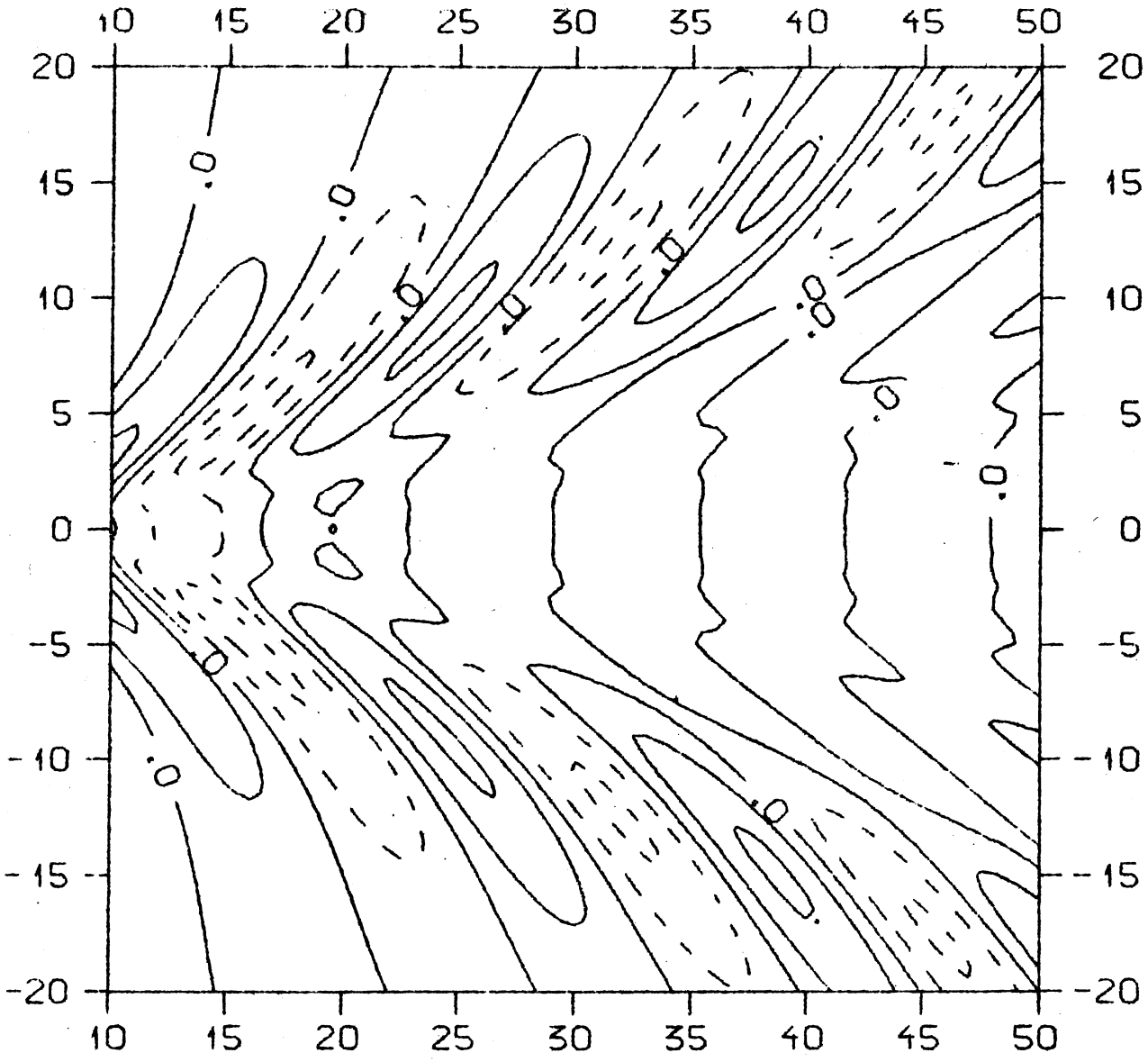

fig. 5.6

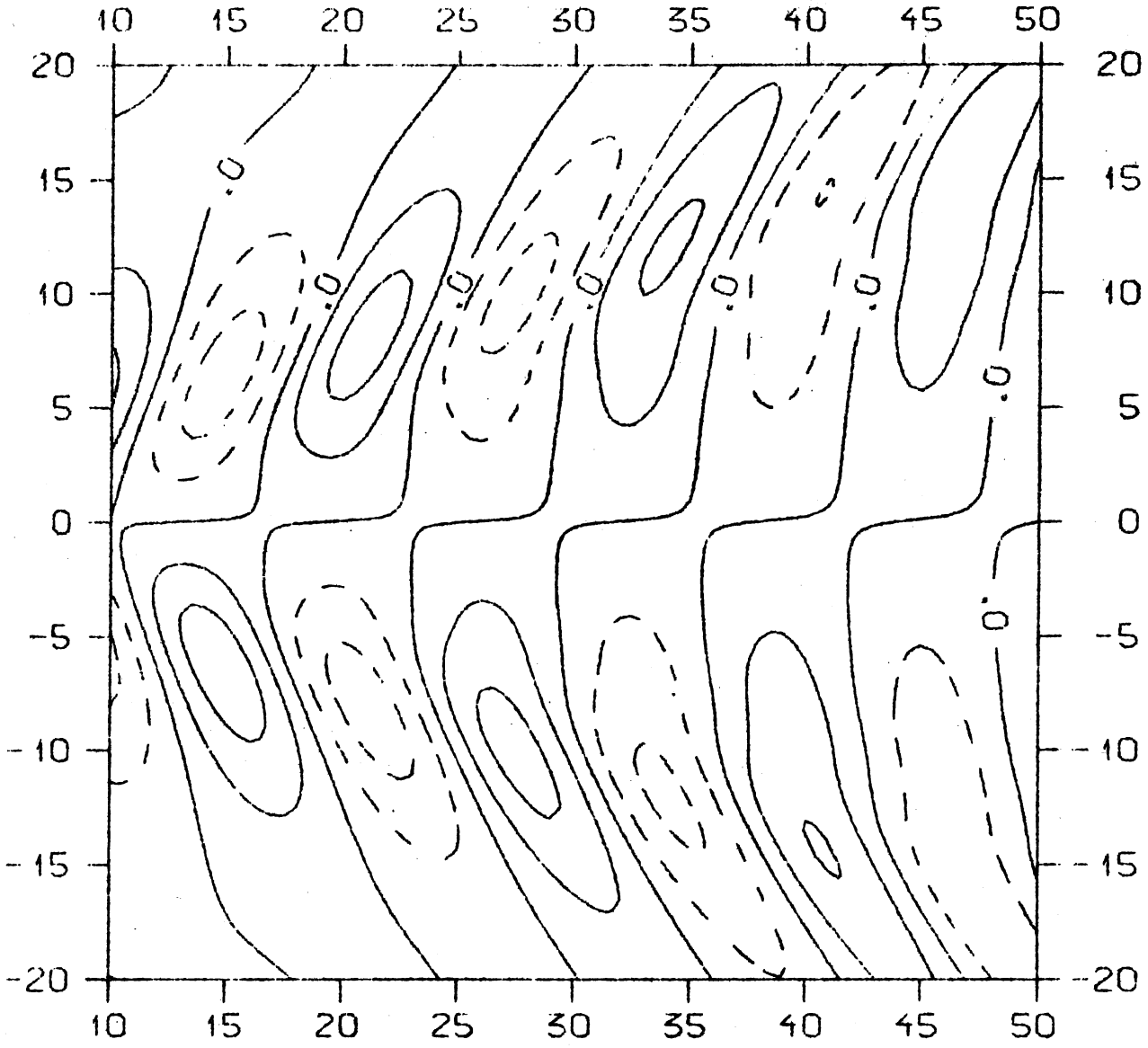

fig. 5.7

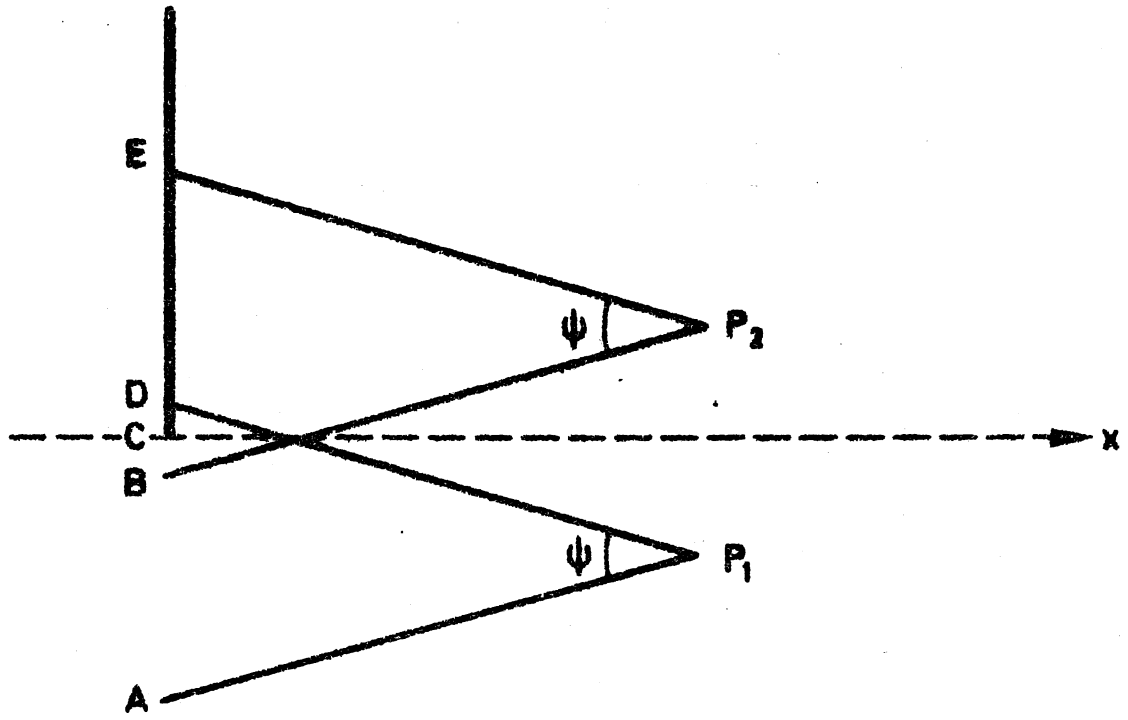

fig. 5.8